# Air oxygen fractionation associated with respiration and photosynthesis processes in plants: impact on the study of the global Dole effect

Clémence Paul, Clément Piel, Joana Sauze, Ji-Woong Yang, Marie Bouchet, Olivier Jossoud, Arnaud Dapoigny, Daniele Romanini, Frédéric Prié, Sébastien Devidal, et al.

# Air oxygen fractionation associated with respiration and photosynthesis processes in plants: impact on the study of the global Dole effect

Clémence Paul[1], Clément Piel[2], Joana Sauze[2], Ji-Woong Yang[1], Marie Bouchet[1], Olivier Jossoud[1], Arnaud Dapoigny[1], Daniele Romanini[4], Frédéric Prié[1], Sébastien Devidal[2], Roxanne Jacob[1], Alexandru Milcu[2,3] and Amaëlle Landais[1]

[1] Laboratoire des Sciences du Climat et de l'Environnement, LSCE/IPSL, CEA-CNRS-UVSQ, Université Paris-Saclay, 91191 Gif-sur-Yvette, France

[2]Ecotron Européen de Montpellier (UAR 3248), Univ Montpellier, Centre National de la Recherche Scientifique (CNRS), Campus Baillarguet, Montferrier-sur-Lez, France

[3]Centre d'Ecologie Fonctionnelle et Evolutive, Univ Montpellier, CNRS, Univ Paul Valéry, EPHE, IRD, Montpellier, France

[4]Laboratoire Interdisciplinaire de Physique, Univ Grenoble Alpes, CNRS/UGA, Saint-Martin-d'Hères, France

Correspondence: Clémence Paul (clemence.paul@lsce.ipsl.fr)

# Abstract

Understanding the global Dole effect (DE) is essential for interpreting variations in the oxygen and water cycles. This study aims at refining the biological fractionation factors during respiration and photosynthesis in terrestrial plants and reassess their impact on the DE. Using multiplexed closed chamber experiments on five C3 and C4 plant species under soil and hydroponic conditions, we quantified isotopic discrimination during respiration (−16 to −21 ‰) and photosynthesis (approximately +3 to +5 ‰). These results confirm a previously reported positive discrimination associated with terrestrial photosynthesis, challenging the assumption of zero fractionation in this process. By incorporating these new estimates into updated calculations obtained using outputs of Earth system models, we obtain variations in DE between the last glacial maximum and the pre-industrial period consistent with ice core data. However, the changes around 6,000 years ago cannot be explained solely by variations in terrestrial and oceanic productivity ratios, reinforcing the role of low-latitude hydrological processes. These results highlight the need to improve quantification of biological fractionation associated with the oxygen cycle in reconstructions of past atmospheric composition.

# 1. Introduction

Air oxygen ($O_2$) is the most abundant element on Earth. Photosynthesis is the biological mechanism by which oxygen is produced by terrestrial and marine organisms, while it is consumed by another process, respiration. The study of isotopic composition of $O_2$ makes it possible to study all the fundamental biogeochemical cycles, in particular those of $O_2$, $CO_2$ and water. The analysis of ancient air trapped in bubbles in ice cores provides a signal of past variations in the ratio of oxygen 18 ($^{18}O$) to oxygen 16 ($^{16}O$) or $\delta^{18}O$ of air $O_2$ (also known as $\delta^{18}O_{atm}$). The $\delta^{18}O_{atm}$ variations can be interpreted as variations in the hydrological cycle at low latitudes and/or as variations of the relative proportion of the oceanic vs terrestrial biosphere productivity (Bender et al., 1994; Luz et al., 1999; Malaizé et al., 1999; Severinghaus et al., 2009; Blunier et al., 2002; Landais et al., 2010; Luz and Barkan, 2011). Several studies have measured the enrichment of $\delta^{18}O_{atm}$ vs. the $\delta^{18}O$ of water of the global ocean (with a value very close to the one of the Vienna Standard Mean Ocean Water, VSMOW) to be 23.5 - 24 ‰ (Dole, 1935; Kroopnick and Craig, 1972; Barkan and Luz, 2005; Pack et al., 2017; Wostbrock and Sharp, 2021). This difference between $\delta^{18}O_{atm}$ and $\delta^{18}O_{sw}$ (sw for sea water) varies with time and is named the Dole effect (DE). Subsequently, several studies have attempted to estimate the various parameters contributing to the Dole effect in order to get as close as possible to this value of 24 ‰ (Bender et al., 1994; Hoffman et al., 2004; Luz and Barkan, 2011) and better understand the processes involved.

Understanding past variations in $\delta^{18}O_{atm}$ and the Dole effect remains a subject of ongoing research. More than 30 years ago, Bender et al. (1994) demonstrated that $\delta^{18}O_{atm}$ varies in phase with precession, establishing its further utility as a dating tool for ice cores (Dreyfus et al., 2007; Bazin et al., 2013; Bouchet et al., 2023). It has been proposed that these isotopic fluctuations are influenced by shifts in the low-latitude hydrological cycle, which impact the isotopic composition of the water consumed by the plants and

transmitted to the atmospheric $O_2$ during photosynthesis (Landais et al., 2010; Seltzer et al., 2017, Extier et al., 2018). One of the strongest lines of evidence for this connection is the close correspondence between $\delta^{18}O_{atm}$ and $\delta^{18}O_{calcite}$ recorded in East Asian speleothems over the past 650,000 years (Cheng et al., 2016; Huang et al., 2020), reflecting the sensitivity of these proxies to monsoonal variability and broader tropical climate dynamics (Wang et al., 2008).

In addition, Bender et al. (1994), Malaizé et al. (1999) and Hoffmann et al. (2004) suggested that variations of the Dole effect are influenced by the relative proportion of terrestrial vs oceanic productivity, an interpretation which was challenged by Luz and Barkan (2011) who proposed that Dole effect is only a marker of variations in the hydrological cycle at low latitudes. The differences between these interpretations is linked to the different estimates of the fractionation factors of the biological processes. Finally, a recent study by Paul et al. (2023) noticed a non-zero discrimination (3.7 ‰) for the terrestrial photosynthesis contradicting the previous experimental determination of Guy et al. (1993). This result again challenges the interpretation of the Dole effect variations.

The terrestrial photosynthetic discrimination evidenced by Paul et al. (2023) needs to be verified since the experiment was carried out on a single plant species. Moreover, this experiment was not performed at the organism scale as in previous studies (Helman et al., 2005; Eisenstadt et al., 2010) but at the scale of the ecosystem, hence involving the presence of soil. While this approach may better reflect reality, other processes occurring during the light period, besides photosynthesis, could influence the determination of the fractionation coefficient during photosynthesis. The first objective of our study is thus to better quantify the discriminations of terrestrial respiration and photosynthesis in closed chambers on a larger number of terrestrial plant species. As a second objective, we revise the interpretation of the Dole effect using the newly estimated fractionation coefficients.

The manuscript is organized as follows. In a first section, we present the general evolution of ideas on the calculation and the interpretation of $\delta^{18}O_{atm}$ and the Dole effect. The second section is devoted to materials and methods, and provides details on the plants and controlled biological chambers used in the study. Modeled gross primary production outputs from Paleoclimate Modelling Intercomparison Project (PMIP) were also used to help interpretation of the global Dole effect. The third section presents the results of biological fractionation coefficients for the different plants. Finally, the last section explores the implications of the newly calculated fractionation coefficients for interpreting the Dole effect.

# 2. State of art: general concept of calculation and interpretation of $\delta^{18}O_{atm}$

## 2.1. Calculations of $\delta^{18}O_{atm}$ and Dole effect

### *2.1.1. The definition of Dole effect*

We follow conventional choice of isotopic standard used in relevant literature: the $\delta^{18}O_{atm}$ is expressed with respect to present-day atmospheric air as a standard. In contrast, $\delta^{18}O_{sw}$ is expressed with respect to the international standard for water: Vienna Standard Mean Ocean Water (V-SMOW). The difference in the $\delta^{18}O$ of $O_2$ value for present-day atmosphere and in the $\delta^{18}O$ of $H_2O$ for the V-SMOW standard is called the Dole effect (DE):

$$\delta^{18}O_{atm} = \delta^{18}O_{sw} + DE \quad (1)$$

The Dole effect is caused by the different processes involved in the oxygen and water cycles, the major $O_2$ fluxes on Earth being photosynthesis and respiration.

The previous studies have decomposed the global Dole effect into an oceanic and terrestrial Dole effect (e.g. Bender et al., 1994; Hoffmann et al., 2004). These two contributions of the Dole effect can be decomposed as:

$$DE_{oceanic\_or\_terrestrial} = \delta^{18}O_{water\ \ biosphere} - \delta^{18}O_{sw} + {}^{18}\varepsilon_{respiration} + {}^{18}\varepsilon_{photosynthesis} \quad (2)$$

Where ${}^{18}\varepsilon_{respiration}$ represents the positive discrimination associated with the respiration of organisms which enriches the isotopic composition of oxygen in the $O_2$ of respired air compared to $O_2$ of atmospheric air and ${}^{18}\varepsilon_{photosynthesis}$ represents the discrimination associated with the photosynthesis of organisms which modifies the isotopic composition of oxygen in the $O_2$ of atmospheric air with respect to the isotopic composition of oxygen in the substrate water. $\delta^{18}O_{water\_biosphere}$ is the $\delta^{18}O$ of the water consumed by the biosphere during photosynthesis and is expressed with respect to V-SMOW.

In the ocean, the $\delta^{18}O_{water\_biosphere}$ is equal to the $\delta^{18}O_{sw}$ and the oceanic Dole effect can directly be expressed as:

$$DE_{ocean} = {}^{18}\varepsilon_{respiration\_ocean} + {}^{18}\varepsilon_{photosynthesis\_ocean} \quad (3)$$

Where ${}^{18}\varepsilon_{respiration\_ocean}$ represents the discrimination associated with the respiration of marine organisms and ${}^{18}\varepsilon_{photosynthesis\_ocean}$ the discrimination between $\delta^{18}O$ of $O_2$ produced and $\delta^{18}O$ of water consumed during the photosynthesis of autotrophic marine organisms.

On the terrestrial biosphere, the source of oxygen for plant photosynthesis is the leaf water. The $\delta^{18}O$ of leaf water is related to the $\delta^{18}O$ of soil water with additional fractionation due to evapotranspiration (Hoffmann et al., 2004; West et al., 2008). The terrestrial Dole effect can be decomposed as follows:

$$DE_{terr} = \delta^{18}O_{soil\_water} - \delta^{18}O_{sw} + {}^{18}\varepsilon_{evapotranspi} + {}^{18}\varepsilon_{respiration\_terr} + {}^{18}\varepsilon_{photosynthesis\_terr} \quad (4)$$

where ${}^{18}\varepsilon_{evapotranspi}$ represents the discrimination during evapotranspiration, ${}^{18}\varepsilon_{respiration\_terr}$ represents the discrimination during the respiration of terrestrial organisms and ${}^{18}\varepsilon_{photosynthesis\_terr}$ represents the discrimination between $\delta^{18}O$ of $O_2$ produced in the atmosphere and $\delta^{18}O$ of water consumed during the photosynthesis of autotrophic terrestrial organisms.

From the definition of the oceanic and terrestrial Dole effects and making the steady state assumption, *i.e.* that the biological fluxes of dioxygen production (photosynthesis) and dioxygen consumption (mainly respiration) are equal, it is possible to express the global Dole effect as:

$$DE_{global} = \frac{GPP_{ocean} \times DE_{ocean} + GPP_{terr} \times DE_{terr}}{GPP_{total}} - {}^{18}\varepsilon_{strat} \quad (5)$$

with $GPP_{ocean}$ corresponding to the gross photosynthetic $O_2$ production rate of the ocean, $GPP_{terr}$ corresponding to the gross photosynthetic $O_2$ production rate of the land, $GPP_{total}$ corresponding to the gross photosynthetic $O_2$ production rate of the ocean and land (i.e. $GPP_{total} = GPP_{ocean} + GPP_{terr}$). $^{18}\varepsilon_{strat}$ is the discrimination of $O_2$ due to photochemical reaction in the stratosphere (Bender et al., 1994) and equals 0.3 ‰.

By simplifying the equation with the parameter $r = \frac{GPP_{ocean}}{GPP_{total}}$, we can write the definition of $DE_{global}$ as follows:

$$DE_{global} = r \times DE_{ocean} + (1 - r) \times DE_{terr} - {}^{18}\varepsilon_{strat} \quad (6)$$

### *2.1.2. The main drivers of Dole effect*

In order to identify the main drivers of the Dole effect, it is necessary to have estimates of the different terms in the equations 3, 4 and 5. The $\delta^{18}O_{mw}$, which is the main factor controlling the $\delta^{18}O_{soil\_water}$, varies temporally and spatially. The temporal variations are partly linked to changes in the $\delta^{18}O_{sw}$, particularly during glacial–interglacial transitions: the buildup of continental ice during glacial period enriches the oceans in heavy isotopes by storing the lighter ones in ice sheets because of the low value of the $\delta^{18}O$ of snow in polar region. The low value of $\delta^{18}O$ of snow in polar region originates from atmospheric processes modifying the isotopic composition of precipitation and leading to a $\delta^{18}O$ decrease toward the high latitudes. As water vapor is transported from the oceanic evaporation source to the precipitation site, successive condensation events cause isotopic fractionation with the heaviest isotopes preferentially found in the condensed phase. Consequently, as air masses move to higher latitudes or to higher elevations, precipitation becomes increasingly depleted in $^{18}O$. This mechanism explains why $\delta^{18}O_{mw}$

values generally decrease with distance from the ocean and latitude relative to evaporation source regions (Aggarwal et al., 2010).

At first approximation, the $\delta^{18}O_{soil\_water}$ can be approximated by the annual average of the $\delta^{18}O_{mw}$ (Anderson et al., 1998; Helliker and Richter 2008). Then, $\delta^{18}O$ of leaf water is enriched with respect to $\delta^{18}O_{soil\_water}$ due to evapotranspiration, the main contribution being the evaporation of water from leaves. This enrichment shows large temporal and spatial variations due to the diversity of leaf types and anatomies as well as to fluctuations in temperature, humidity and surrounding water vapor $\delta^{18}O$ (*e.g.* Flanagan et al., 1991; Cernuzak et al., 2016). Despite strong spatial variability, measurements of $\delta^{18}O$ of $CO_2$ led to an estimate of the global value of 7 ‰ for the difference between $\delta^{18}O_{lw}$ (lw = leaf water) and $\delta^{18}O_{sw}$ for present-day (Gillon and Yakir, 2001; West et al., 2008).

The value for ${}^{18}\varepsilon_{respiration}$ should be calculated considering the different biological processes consuming $O_2$. Bender et al. (1994) listed three main processes which should be considered both in the terrestrial and oceanic biosphere: dark respiration, Mehler reaction and photorespiration. For the first estimate of ${}^{18}\varepsilon_{respiration\_terr}$ (18.0 ‰), Bender et al. (1994) used the most recent values observed for dark respiration, Mehler reaction and photorespiration from biological experiments driven at the scale of the enzyme or the cell (Guy et al., 1992, 1993). For the first estimate of ${}^{18}\varepsilon_{respiration\_ocean}$ (18.9 ‰), Bender et al. (1994) used concentrations and $\delta^{18}O$ of dissolved $O_2$ from sea water samples or from biological experiments performed on several marine organisms (e.g. bacteria, microalgae, copepods). Over the years, these estimates were refined using studies performed at the cellular scale (Helman et al., 2005) or at broader scale (Angert et al., 2003; Hendricks et al., 2004; Levine et al., 2009; Luz and Barkan 2011; Wurgaft et al., 2022; Kim and Kang, 2024).

As for the $^{18}\varepsilon_{photosynthesis\_ocean}$, the first studies detected no discrimination (Guy et al., 1989, studies on cyanobacteria -*Anacystis nidulans* - and diatoms - *Phaeodactylum tricornutum* -; Vinogradov et al., 1959 studies on samples of aquatic populations in the Bay of Bengal; Helman et al., 2005 studies on cyanobacteria *Synochocystis*). However, more recently, Eisenstadt et al. (2010), studied a diversity of marine organisms (phytoplankton) and found a non-zero photosynthetic discrimination for eukaryotic algae: 4.5 ‰ for *Phaeodactylum tricornutum* diatoms, 3 ‰ for *Nannocloropsis sp.* diatoms, 5.5 ‰ for Coccolithophores *Emiliania huxleyi* and 7 ‰ for *Chlamydomonas oreinhardtii*. A non-zero value for the photosynthetic discrimination is difficult to explain either from the physiological point of view (Tcherkez and Farquhar, 2007) or by the diffusion during the production of $O_2$ and then the diffusion in the free air ($^{16}O^{16}O$ is diffusing more rapidly than $^{18}O^{16}O$ so that we should have measured an apparent negative discrimination during photosynthesis). Eisenstadt et al. (2010) ruled out the existence of large $O_2$ consumption reaction fractionating $O_2$ during their experiments because there was no $O_2$ in their experimental environment. Paul et al. (2023) performed controlled experiments with fescue for the terrestrial photosynthesis and found a first value of 3.7 ‰ for $^{18}\varepsilon_{photosynthesis\_terr}$.

### *2.1.3. Different estimates of Dole effect*

In their first estimates of the terrestrial and oceanic Dole effects (Table 1), Bender et al. (1994) used the global estimates available at the time and found a significantly lower value for the oceanic Dole effect compared to the continental Dole effect (Fig. 2). Hoffmann et al. (2004) revisited this first calculation through a different integration of the isotopic effects: they used various models (an atmospheric general circulation model equipped

with water isotopes, a model of vegetation and an ocean model with a module for biological productivity) to calculate spatial variations of $\delta^{18}O_{mw}$, $\delta^{18}O_{lw}$, ${}^{18}\varepsilon_{respiration}$ and biological fluxes before global integration. This model was then used and updated by Ciais et al. (2012) for an application comparing the last glacial maximum (LGM) and pre-industrial (PI). They confirmed the results of Bender et al. (1994) that the oceanic Dole effect should be lower than the terrestrial one and even found a much larger difference between these two contributions (Table 1). If the terrestrial and oceanic Dole effects are significantly different (Fig. 2), it is then expected that the change in the relative proportion of the terrestrial and oceanic productivities is one of the main drivers of the variations of the global Dole effect as measured in climatic archives.

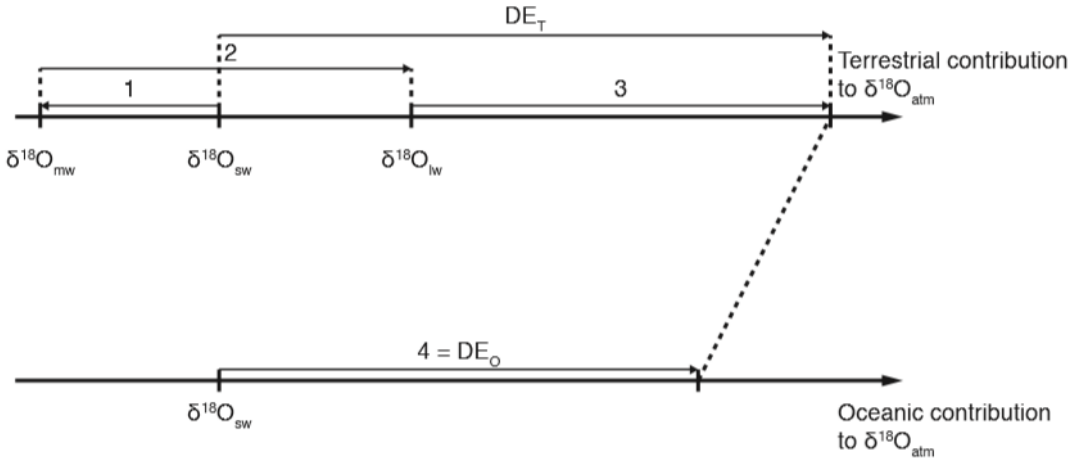


*Figure 2. Diagram of the main contributions to $\delta^{18}O_{atm}$. (1) Fractionation of water during evaporation and precipitation. (2) Fractionation of water during evapotranspiration. (3) Fractionation of atmospheric oxygen during terrestrial respiration (4) Fractionation of atmospheric oxygen during oceanic respiration. (5) Fractionation during oceanic photosynthesis. $DE_T$ = terrestrial Dole effect and $DE_O$ = oceanic Dole effect (from Landais et al., 2007).*

Using latest estimates of ${}^{18}\varepsilon_{respiration}$ and ${}^{18}\varepsilon_{photosynthesis}$, Luz and Barkan (2011) found a different result: $DE_{terr}$ and $DE_{ocean}$ are equal to about 24 ‰ each (Fig. 3). The difference between this result and the previous results of Bender et al. (1994) and Hoffmann et al.

(2004) is due to their estimate of (1) $^{18}\varepsilon_{respiration\_terr}$ being smaller than previous estimates because of the diffusion in the soil and (2) $^{18}\varepsilon_{photosynthesis\_ocean}$ estimated to 6 ‰ instead of 0 ‰ in the first calculations. In this case (Fig. 3), the relative proportion of terrestrial and oceanic productivities cannot explain the variations of the global Dole effect which are expected to be simply the result of variations in monsoon cycles leading to variations in the $\delta^{18}O_{mw}$ and $\delta^{18}O_{lw}$ (Luz and Barkan, 2011; Landais et al., 2010).

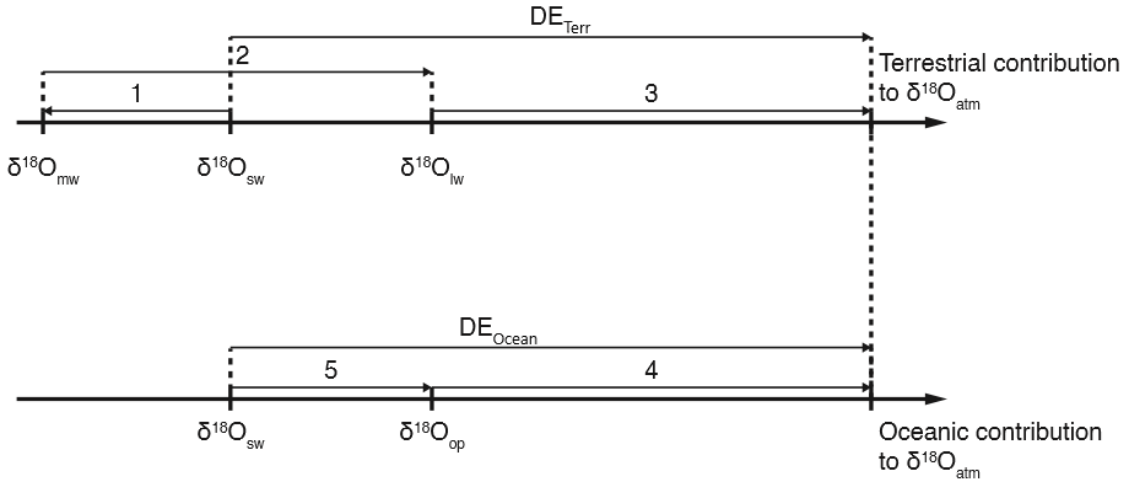


*Figure 3. Diagram of the main contributions to $\delta^{18}O_{atm}$. (1) Fractionation of water during evaporation and precipitation. (2) Fractionation of water during evapotranspiration. (3) Fractionation of atmospheric oxygen during terrestrial respiration. (4) Fractionation of atmospheric oxygen during oceanic respiration. (5) Fractionation during oceanic photosynthesis ($\delta^{18}O_{op}$). $DE_{Terr}$ = terrestrial Dole effect and $DE_{Ocean}$ = oceanic Dole effect (modified from Landais et al., 2007).*

The most recent estimate of a terrestrial photosynthetic discrimination is equal to 3.7 ‰ (Paul et al., 2023). It was validated by a second study with a multiplexed system (Paul et al., 2025). These results would again increase the terrestrial Dole effect making it larger than the oceanic one.

*Table 1. (a) Parameters used to calculate oceanic, terrestrial and the current global Dole effects in literature. *reference given in the title of the column, [1]Farquhar et al. (1980); [2]Keeling and Shertz (1992); [3]Kiddon et al. (1993); [4]Farquhar et al. (1993); [5]Guy et al. (1992), (1993); [6]West et al. (2008) and Benson and Krause (1984); [7]Landais et al. (2007). (b) Calculation of the Dole effects (oceanic, terrestrial and global). LGM = Last Glacial Maximum and PI = pre-industrial*

| | Bender et al. (1994) | Hoffmann et al. (2004) | Luz and Barkan (2011) |
|---|---|---|---|
| | | Present | |
| GPP-$O_2$ ocean (Pmol $O_2$/yr) | 12[1] | 7.6* | |
| GPP-$O_2$ land (Pmol $O_2$/yr) | 20.4[2] | 16.79* | |
| $^{18}\varepsilon_{respiration\_ocean}$(‰) | 18.9[3] | 20[3] | 19.7* |
| $^{18}\varepsilon_{photosynthesis\_ocean}$(‰) | 0[5] | 0[5] | 4[5] |
| $\delta^{18}O_{lw}$(‰) | 4.4[4] | 6* | 5.7[6] |
| $^{18}\varepsilon_{respiration\_terr}$(‰) | 18[5] | 20[3] | 17.7[7] |
| $^{18}\varepsilon_{photosynthesis\_terr}$(‰) | 0[5] | 0[5] | 0[5] |

b)

| | Bender et al. (1994) | Hoffmann et al. (2004) | Luz and Barkan (2011) | Ciais et al. (2012) | |
|---|---|---|---|---|---|
| | | | Present | PI | LGM |
| $DE_{ocean}$(‰) | 18.9 | 16.9 | 23.5 | 19.8 | 20 |
| $DE_{terr}$(‰) | 22.4 | 26.9 | 23.5 | 28.3 | 29.5 |
| $DE_{global\_calculated}$(‰) | 20.8 | 23.5 | 23.2 | - | - |

## 2.2. The evolution of the Dole effect over the last deglaciation

Figure 4 shows the evolution of the Dole effect calculated using different datasets and age models from the Last Glacial Maximum (LGM) (20 ka BP) to the Pre-Industrial period (PI). For the $\delta^{18}O_{atm}$ we used the high resolution (100 years on average) record from the WAIS Divide ice core (Seltzer et al., 2017). For the oceanic $\delta^{18}O$, the three following series were used: (i) the benthic $\delta^{18}O$ stack of Lisiecki and Raymo (2005) whose age model is tuned to the EPICA Dome C ice core timescales (Parrenin et al., 2007; Veres et al., 2013; Bouchet et al., 2023), (ii) the benthic $\delta^{18}O$ volume-weighted stack of Lisiecki and Stern (2016) on its original radiocarbon age scale and (iii) the ice-sheet contribution of the oceanic $\delta^{18}O$ modeled by Bintanja et al. (2005). These three curves are then scaled between a value of $\delta^{18}O_{sw}$ of 0 ‰ at PI and of 1 ‰ at LGM (Duplessy et al., 2002; Schrag et al., 2002). We calculate the three resulting scenarios for the Dole effect fluctuations following this approach. Finally, we also present the alternative Dole effect (DE*) suggested by Huang et al. (2020) in Fig. 4 (pink line). Indeed, Huang et al. (2020) argued that it may be more appropriate to use a stack for sea surface term $\delta^{18}O_{surf}$ rather than the mean oceanic water $\delta^{18}O$ to calculate the Dole effect. We

Although all DE estimates are approximately equal to zero at LGM and PI, they undergo significant fluctuations between -0.4‰ to +0.6 ‰ over the last deglaciation, from 20 to 11 ka BP. The variations observed during this period are inconsistent and diverge from one estimate to another by up to 0.5 ‰. These differences can be attributed to differences in chronology or estimate of the $\delta^{18}O_{sw}$ and we thus avoid interpreting the variation of the DE over this period.

By contrast, all DE and DE* scenarios well agree over the last 10 ka BP time interval and indicate an excursion of 0.4 ‰ towards negative values at 6 ka BP. This deviation is driven by the ice core $\delta^{18}O_{atm}$ signal while $\delta^{18}O_{sw}$ stays stable over this period (panel c).

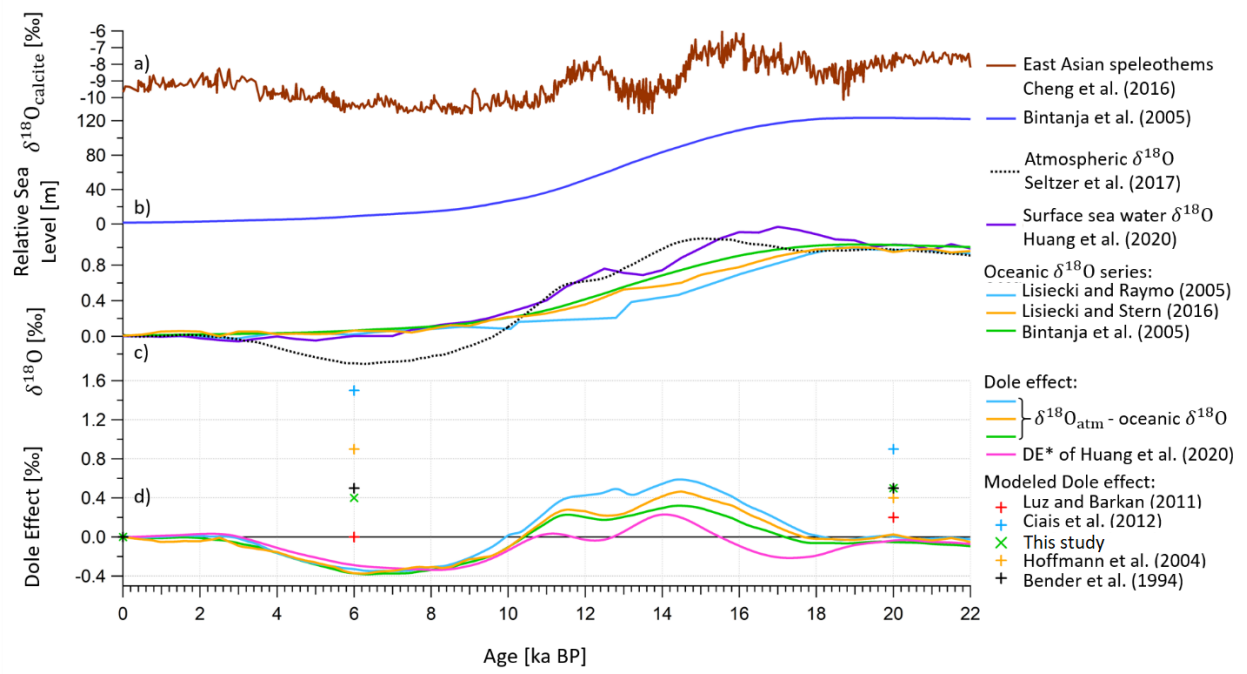


*Figure 4. Different Dole effect scenarios calculated using marine and ice core $\delta^{18}O$ data between 22 and 0 ka BP. a) Uranium-Thorium-dated $\delta^{18}O_{calcite}$ from speleothems of Hulu and Sambao caves (Cheng et al., 2016). b) Sea level relative to PI (Bintanja et al., 2005). c) $\delta^{18}O$ series: $\delta^{18}O_{atm}$ from WAIS Divide ice core on WD2014 age model (black dotted line) (Seltzer et al., 2017; Sigl et al. 2016) and surface sea water $\delta^{18}O$ global stack on its radiocarbon age model (purple line) (Huang et al., 2020). The five oceanic $\delta^{18}O$ series: (i) the benthic $\delta^{18}O$ from the LR04 global stack (Lisiecki and Raymo, 2005) synchronized to the ice core age scale (blue line, Antarctic Ice Core Chronology 2023) (Parrenin et al., 2007; Bouchet et al., 2023), (ii) the benthic $\delta^{18}O$ from the LS16 global stack on its radiocarbon age model (orange line) (Lisiecki and Stern, 2016) and (iii) the modeled ice-sheet contribution to oceanic $\delta^{18}O$ (green line) (Bintanja et al., 2005). The benthic $\delta^{18}O$ data have been scaled between 0 (PI) and 1 ‰ (LGM) values (see text). d) The five scenarios of Dole effect calculated as per $\delta^{18}O_{atm}$ - oceanic $\delta^{18}O$ for the five oceanic $\delta^{18}O$ series (same colors) and the DE* of Huang et al. (2020) (pink line). The crosses indicate the difference with respect to the PI period of the Dole effect at 6 ka and LGM as estimated by the different previous studies as summarized in Table 8.*

# 3. Material and Methods

## 3.1. Study of oxygen isotope fluxes in multiplexed closed chambers on a variety of C3 and C4 plants

### *3.1.1. Plant species*

Different plant species were chosen for the determination of the oxygen fractionation coefficients associated with respiration and photosynthesis (Table 2): *Musa acuminata*, *Nerium oleander*, *Cupressus* sp., *Festuca arundinacea*, and *Zea mays*. The first selection criterion was to use model plants (fescue and maize) that were no taller than 50 cm to fit into the biological chamber with the soil. In addition, plants adapted to different climates (temperate and tropical) and plants with different anatomical characteristics were selected. A comparison between C3 and C4 plants was also considered. In C4 plants, photorespiration is strongly suppressed by a biochemical $CO_2$-concentrating mechanism that elevates $CO_2$ levels around Rubisco in the bundle sheath cells, thereby minimizing oxygenation reactions. In contrast, C3 plants lack this mechanism and are therefore more affected by photorespiratory losses.

*Table 2. Characteristics of the five plants studied in the biological experiments.*

| Scientific name of the plant | Common name of the plant | Climate | Characteristic | Photosynthesis strategy |
|---|---|---|---|---|
| *Festuca arundinacea* | Fescue | Temperate | Herbaceous plant | C3 |
| *Nerium oleander* | Laurel | Temperate - warm | Broadleaved evergreen shrub | C3 |
| *Musa acuminata* | Banana tree | Tropical | Broadleaved evergreen herbaceous plant | C3 |

| | | | | |
|---|---|---|---|---|
| *Cupressus sp.* | Cypress | Temperate-cold | Needleleaved evergreen tree | C3 |
| *Zea mays* | Maize | Tropical | Broadleaved summergreen herbaceous plant | C4 |

365

366 *3.1.2. Set-up of the study of the oxygen isotope fluxes on terrestrial plants in closed chambers*
367

368 3.1.2.1. General strategy for experiments
369

370 We present here the general strategy for experiments carried out on maize, fescue, laurel,
371 banana tree, and cypress grown on a typical compost soil (*Terreau universel*, Botanic,
372 France) whose composition consisted of black and blond peat, wood fiber, green compost
373 and vermicompost, organic and organo-mineral fertilizers, and micronutrient fertilizers).

374 These [soil + plant] experiments conducted in three parallel closed biological chambers
375 (see description below) lasted between three and six days, alternating between dark and
376 light periods (except for the cypress, which only had one dark period), as detailed in Table
377 3.

378 In addition to soil experiments, we chose to grow two plants in hydroponic conditions:
379 maize and fescue (maize 2 and fescue 2 in Table 3). This approach allowed us to eliminate
380 the soil fractionation factor in our calculations.
381 During our experiment series, we also conducted an experiment using soil only. In Paul et
382 al. (2023), the fractionations associated with respiration in the artificial soil used were
383 shown to be similar to natural values reported by Angert et al. (2001), i.e., approximately
384 12 ‰. Because this soil is a good analog for natural soil, we kept the same type of soil for
385 the multiplexing experiments presented here.

386

*Table 3. Experimental conditions for the five plants species studied: experiment references for fescue and maize (1 for experiment 1 with soil and 2 for experiment with hydroponic conditions) and laurel, banana tree, cypress with soil and soil only. * = the lack of data for fescue in hydroponic conditions is the result of a leakage problem encountered at the end of the experiment during the last day period. X = the lack of data for cypress in light periods is the result of a very small $O_2$ fluxes.*

| Plant | Duration of all experiment (day) | Day 1 duration (hour) | Night 1 duration (hour) | Day 2 duration (hour) | Night 2 duration (hour) | Day 3 duration (hour) | Analysis strategy |
|---|---|---|---|---|---|---|---|
| Fescue 1 + soil | 6 | 7 | 65 | 7 | 65 | 7 | IRMS |
| Laurel + soil | 4 | 7 | 19 | 11 | 21 | 11 | IRMS |
| Banana tree + soil | 6 | 7 | 66 | 7 | 65 | 8 | IRMS |
| Maize 1 + soil | 3 | 9 | 19 | 11 | 24 | 12 | IRMS |
| Cypress + soil | 5 | X | 98 | X | X | X | IRMS |
| Soil | 4 | | 97 | | | | IRMS |
| Fescue 2 + soil | 5 | 10 | 27 | 11 | 27 | 13 | IRMS + OF-CEAS |
| Fescue 3 hydroponic | 4 | 23 | 31 | 24 | 22 | * | OF-CEAS |
| Maize 2 with soil | 6 | 5 | 38 | 6 | 57 | 10 | IRMS + OF-CEAS |
| Maize 2 hydroponic | 5 | 10 | 54 | 9 | 57 | 7 | IRMS + OF-CEAS |

### 3.1.2.2. Set-up of the multiplexed chambers

The general setup of the experiments was equivalent to that referred to in Paul et al. (2025) and as detailed below.For each plant study (fescue, laurel, banana, maize, cypress, and soil only), we used three biological chambers simultaneously.

The set of three airtight, transparent, welded polycarbonate chambers (120 L volume) was adapted from the chamber described in Paul et al. (2023) and Milcu et al. (2013). The main controlled environmental parameters inside the closed chambers were temperature, light intensity, $CO_2$ concentration, relative humidity, and differential pressure. Each chamber was used as a closed gas exchange system and was placed in a separate controlled-environment growth chamber in the Microcosms experimental platform of the Montpellier European Ecotron. A multiplexing system had been built to handle the three chambers in parallel (Paul et al., 2025). With this setup, we continuously measured the isotopic composition of $O_2$ using an online optical spectroscopy instrument based on Optical Feedback Cavity Enhanced Absorption Spectroscopy (OF-CEAS) (Piel et al., 2024).

As in Paul et al. (2025), we also obtained IRMS measurements using a flanged air recovery system. In the studies of plants with soil, referred to as fescue 1, laurel, banana tree, maize 1, and cypress in Table 3, we could not use the optical spectrometry analyzer system, as the instrument was under repair.

In the different studies performed with the optical spectrometer, we did two-point calibrations using two reference gases once every day. Because the measured difference in isotopic and elemental composition between the two reference gases was very stable over days, we used only one reference gas calibration (dry atmospheric air) during the day. The measurement sequence was the following:

- 6 min of measurement of atmospheric air - 6 min of measurement of air in chamber 1. This sequence was then applied to each of the three chambers and a full sequence lasted 36 min for the three chambers.

Finally, the analysis of leaf water was performed following the procedure described by Paul et al. (2023). The leaves were collected at the end of each experiment, water extracted by cryogenic trapping under vaccum and extracted water transformed to $O_2$ through a fluorination line (Barkan and Luz, 2005) and $O_2$ analysed by IRMS. Each water sample was processed at least twice leading to an uncertainty of 0.1 ‰ on the $\delta^{18}O$ value.

#### 3.1.2.3. Hydroponic cultivation

For maize, 15 seeds per Petri dish were placed on crushed clay beads (which had been previously washed with bleach to avoid contamination by bacteria, fungi, or algae). The Petri dishes were placed in the dark. After two days, the seeds had germinated, and their roots were sufficiently developed for hydroponic cultivation. The seeds were transplanted into Eppendorf tubes (1 cm in diameter) with the bottom cut off. The Eppendorf tubes were then inserted through a polystyrene plate (L × P × H = 340 × 240 × 7 mm) previously drilled with 12 holes divided into four rows of three holes along its length. This polystyrene plate rested on the surface of a 12 L plastic tray filled with 10 L of nutrient solution. The roots were in permanent contact with the nutrient solution, and the maize plants grew above the polystyrene support to reach a height of around 30 cm after a cultivation period of one month. Germination and growth times were similar to those for growing maize plants in soil. The nutrient solution was changed twice a week.

For fescue, seeds were spread over the surface of plastic garden pots (L × D × H = 70 × 70 × 80 mm). The pots were filled with sand previously rinsed with diluted bleach. The pots were grouped by 12 and placed in plastic basins (L × D × H = 290 × 440 × 70 mm)

447 containing nutrient solution. The pots were irrigated by capillary action through the sand,
448 and the nutrient solution was renewed twice a week to prevent bacterial contamination
449 and algae growth. The seeds germinated, and the fescue plants grew on the sand for
450 about one month. Once the fescue plants were sufficiently robust (strands of around 10
451 cm), the intertwined roots formed a clod of fescue that was easier to handle than a single
452 strand. The clods were removed from their pots, and the roots were plunged into a tub of
453 osmosis water before being rinsed to remove all the sand. The root balls were then
454 transplanted into the hydroponics tank through a polystyrene plate (L × D × H = 360 ×
455 260 × 7 mm). This polystyrene plate, pierced with 12 square holes (15 × 15 mm), could
456 accommodate 12 fescue clods. This plate rested on the surface of a 9 L plastic tray (W ×
457 D × H = 400 × 300 × 100 mm) containing nutrient solution. The nutrient solution was
458 changed twice a week, and the growing time in the nutrient solution (roots in contact with
459 it) lasted about two weeks to one month.

460 As the plants grew in the nutrient solution, an aquarium pump (Brand: Nicrew/model
461 YDQB4105) was connected to a bubbler, which was placed in the solution to oxygenate
462 the aqueous medium.

463 The nutrient solution was produced using 11 powders (Sigma/Aldrich) and osmosed
464 water. A first one-liter stock solution was produced by mixing powders 2 to 11 (Table 4)
465 in 1 L of aqueous solution (osmosis water) in a volumetric flask. The concentrations of
466 each chemical element were given in Table 4 for this first solution produced. The maize
467 stock solution was four times more concentrated for all elements. Next, a dilution was
468 made: 12.5 mL of fescue stock solution was mixed in a 5 L Erlenmeyer flask filled with
469 osmosis water, and 5 mL of maize stock solution in a 5 L Erlenmeyer flask. Concentration
470 stock solution values were given in Table 4. Calcium nitrate powder no.1 (7.08 g for the
471 maize stock solution and 1.77 g for the fescue stock solution) was mixed into the solution
472 at this point, as otherwise this powder would not have dissolved in the first stock solution.

These working solutions were then placed in the trays where the plants were deposited. For fescue, 7.5 L of daughter solution in the 9 L tub, and for maize, 10 L of daughter solution in the 12 L tub. Hydroponics experiments lasted between four and six days (Table 3).

*Table 4. Composition of the 11 powders and concentrations stock solution for fescue and maize*

| No. Powder | Chemical formula | Name | Concentration stock solution fescue (mM) | Concentration stock solution maize (mM) |
|---|---|---|---|---|
| 1 | $Ca(NO_3)_2$, 4 $H_2O$ | Calcium nitrate tetrahydrate | 1.5 | 6 |
| 2 | $KNO_3$ | Potassium nitrate | 1.25 | 5 |
| 3 | $KH_2PO_4$ | Potassium phosphate monobasic | 0.5 | 2 |
| 4 | $MgSO_4$, 7 $H_2O$ | Magnesium sulfate heptahydrate | 0.75 | 3 |
| 5 | $Na_2SIO_3$, 5 $H_2O$ | Sodium metasilicate pentahydrate | 0.1 | 0.4 |
| 6 | Na-Fe-EDTA | $C_{10}H_{12}N_2NaFeO_8$ | 0.05 | 0.2 |
| 7 | $H_3BO_3$ | Boric acid | 0.05 | 0.2 |
| 8 | $MnSO_4$, $H_2O$ | Manganese sulfate monohydrate | 0.012 | 0.048 |
| 9 | $ZnSO_4$, 7 $H_2O$ | Zinc sulfate heptahydrate | 0.001 | 0.004 |
| 10 | $CuSO_4$, $5H_2O$ | Copper sulfate pentahydrate | 0.0007 | 0.0028 |
| 11 | $Na_2MoO_4$, 2 $H_2O$ | Sodium molybdate dihydrate | 0.00024 | 0.00096 |

## 3.2. Quantification of fractionation factors associated with respiration and photosynthesis processes

In order to calculate the fractionation factors associated with dark respiration and photosynthesis of soil and plants, we use the following equations 6 and 8 (for details, refer to Paul et al., 2023).

The isotopic discrimination for dark respiration, ${}^{18}\varepsilon_{dark\_respi}$ corresponding to the depletion of the $O_2$ consumed by the plant with respect to the $O_2$ in the atmosphere is given by:

$$ {}^{18}\varepsilon_{dark\_respi} = {}^{18}\alpha_{dark\_respi} - 1 = \frac{ln\left(\frac{\delta^{18}O_t+1}{\delta^{18}O_{t0}+1}\right)}{ln\left(\frac{n(O_2)_t}{n(O_2)_{t0}}\right)} \quad (6) $$

where ${}^{18}\varepsilon_{dark\_respi}$ is the dark respiration fractionation factor, t0 is the starting time of each dark period and t is the time at the given moment. $n$ is the number of moles of $O_2$ containing $^{18}O$ or $^{16}O$.

$\frac{n(O_2)_t}{n(O_2)_{t0}}$ is linked to $\delta\left(\frac{O_2}{N_2}\right)$ as:

$$ \frac{n(O_2)_t}{n(O_2)_{t0}} = \frac{\frac{\delta\left(\frac{O_2}{N_2}\right)_t}{1000}+1}{\frac{\delta\left(\frac{O_2}{N_2}\right)_{t0}}{1000}+1} \quad (7) $$

Photosynthesis isotopic discrimination, ${}^{18}\varepsilon_{\text{photosynthesis}}$, is calculated as:

$$ {}^{18}\alpha_{photosynthesis} = \frac{n(O_2)_t \,/\, n(O_2)_{t0} \times a^{18}R + {}^{18}R_t \times \left( F_{photosynthesis} - F_{total\_respi} + {}^{18}\alpha_{total\_respi} \times F_{total\_respi} \right)}{{}^{18}R_{lw} \times F_{photosynthesis}} \quad (8) $$

where, ${}^{18}R$ is the ratio of the concentration ${}^{18}R = \frac{n({}^{18}O)}{n({}^{16}O)}$, $a{}^{18}R = \frac{d{}^{18}R}{dt}$, during the light period, $F_{photosynthesis}$ and $F_{total\_respi}$ are, respectively, photosynthesis and consumption fluxes of oxygen. *lw* stands for leaf water.

${}^{18}\alpha_{photosynthesis}$ depends on the values of ${}^{18}\alpha_{total\_respi}$ and of $F_{total\_respi}$, themselves depending on the values of ${}^{18}\alpha_{Mehler}$ (fractionation factor associated with Mehler reaction), $F_{Mehler}$ (flux of oxygen related to Mehler reaction), ${}^{18}\alpha_{dark\_respi}$, $F_{dark\_respi}$, ${}^{18}\alpha_{photorespi}$ (fractionation factor associated with photorespiration) and $F_{photorespi}$ (photorespiration flux of oxygen) as:

$$ {}^{18}\alpha_{total_{respi}} = {}^{18}\alpha_{photorespi} \times f_{photorespi} + {}^{18}\alpha_{Mehler} \times f_{Mehler} + {}^{18}\alpha_{dark\_respi} \times f_{dark\_respi} \quad (9) $$

with,

$$ f_{dark\_respi} + f_{photorespi} + f_{Mehler} = 1 \quad (10) $$

and,

$$ \frac{F_{dark\_respi}}{F_{total\_respi}} = f_{dark\_respi} \quad (11) $$

$f$ indicates the fraction of the total oxygen uptake flux corresponding to each process (dark respiration, photorespiration and Mehler reaction).

Because maize is a C4 plant, we consider that photorespiration and Mehler reaction were not involved in the $O_2$ consumption by the plant (Laisk and Edwards, 1997) which makes calculations of ${}^{18}\varepsilon_{photosynthesis}$ easier ($f_{Mehler}$ and $f_{photorespi}$ are equal to 0).

For C3 plants, we need to consider photorespiration and Mehler reactions. In the absence of further constraints, we used here, as first approximation and as in Paul et al. (2023), the global values from Landais et al. (2007) for $f_{dark\_respi}$ (0.6), $f_{photorespi}$ (0.3) and $f_{Mehler}$ (0.1). Values for ${}^{18}\varepsilon_{photosynthesis}$ and ${}^{18}\varepsilon_{Mehler}$ were based on the most recent estimates of Helman et al. (2005). The initial value for photorespiration isotopic discrimination is - 21.3 ‰ for ${}^{18}\varepsilon_{photorespi}$ as given by Helman et al. (2005). For the Mehler reaction we also chose the value proposed by Helman et al. (2005): ${}^{18}\varepsilon_{Mehler}$ = - 10.8 ‰.

## 3.3. Global GPP-$O_2$ calculations using model outputs

To estimate the Dole effect variations with time, we calculate the global GPP-$O_2$ in terrestrial and oceanic biospheres using the outputs of Paleoclimate Modelling Intercomparison Project (PMIP) simulations. We use the IPSL-CM5A (PMIP3), MIROC-ESM (PMIP3), and MIROC-ES2L (PMIP4) models since these provide both land and ocean biogeochemistry results for PI, mid-Holocene (MH) 6 ka BP, and LGM experiments. These results are available for download on the Earth System Grid Federation (ESGF) database (https://aims2.llnl.gov/search).

The global mean GPP-$O_2$ is calculated from PMIP outputs following the methodologies described by Blunier et al. (2002) with some modification. For the terrestrial biosphere, the models calculate the gross carbon productivity (GPP-C) of each plant functional type

(PFT). The modelled global GPP-C is partitioned between GPP-C by C3 plants and GPP-C by C4 plants. The Earth System Models usually have one or two PFT of C4 grass. We therefore partition GPP-C by C3 and GPP-C by C4 plants by assuming that all PFTs other than C4 grass are C3 plants. A portion of photosynthetic production of $O_2$ in the C3 plants is consumed via photorespiration. Here we assume no photorespiration in C4 plants. To estimate the GPP-C of C3 plants without consumption by photorespiration, the ratio of total (*i.e.*, dark respiration and photorespiration) to dark respiration is multiplied by the GPP-C of C3 plants. Following von Caemmerer and Farquhar (1981), this ratio is calculated as following:

$$\frac{Dark\ respiration + Photorespiration}{Dark\ respiration} = \frac{4.5}{4} \times \frac{C_i + (7/3) \times \Gamma_*}{C_i - \Gamma_*} \quad (16)$$

where $C_i$ is the partial pressure of $CO_2$ inside the leaf and $\Gamma_*$ is the $CO_2$ compensation point. To calculate $C_i$, we assume a constant ratio (0.65) of $C_i$ following Blunier et al. (2002). The $CO_2$ compensation point is calculated according to the following equation by Prentice et al. (2017) to account for temperature changes:

$$\Gamma_* = 42.75 \times exp\left[\frac{37830}{8.314} \times \left(\frac{1}{298} - \frac{1}{T_K}\right)\right] \quad (17)$$

here $T_K$ is temperature in Kelvin, and is taken from the simulated 2-meter air temperature by the models, 8.314 is the universal gas constant (R in J $mol^{-1}$ $K^{-1}$) and 37,830 is the activation energy (in J $mol^{-1}$). The resulting ratio of dark respiration and photorespiration to dark respiration is ranging between 1.9 and 2.4 depending on the model used and the boundary conditions. The GPP-C is converted to GPP-$O_2$ by multiplying the

photosynthetic quotient of 1.07 (Keeling, 1988). To consider the Mehler reaction, the GPP-$O_2$ is then divided by 0.9 assuming a constant fraction (10 %) of Mehler reaction in the consumption of $O_2$.

The marine biogeochemistry components of the PMIP models do not calculate marine GPP-$O_2$. Instead, we calculate the marine GPP-$O_2$ from the simulated net primary productivity in terms of carbon (NPP-C) by multiplying by 2.7, the ratio of $^{18}$O-based GPP-$O_2$ (measured by incubation with $^{18}$O-labelled water) to $^{14}$C-based primary production rate (measured by incubation with $^{14}$C-labelled bicarbonate) found in the compilation of the JGOFS (Joint Global Ocean Flux Study) measurements (Marra, 2002).

# 4. Results

## 4.1. Study of oxygen isotopes fractionation factors in multiplexed closed chambers on a variety of C3 and C4 plants

We present here the discrimination associated with dark respiration and photosynthesis of experiments carried out on fescue, banana tree, laurel and cypress with soil and maize and fescue in hydroponic conditions (Table 5).

*Table 5. Average and standard deviation of the isotopic discriminations for different biological processes for 5 different plant species with soil (Fescue, Banana tree, Laurel, Cypress and Maize) and 2 different plant species under hydroponic conditions (Maize and Fescue). Isotopic compositions were analyzed by IRMS. X = no light period, thus no $^{18}\varepsilon_{photosynthesis}$ value for cypress experiment (see explanation on Table 3). X* = the lack of data for fescue in hydroponics is the result of a leakage problem (at the level of the sampling of the flask system) encountered at the end of the experiment for the last day period. The standard deviation is given by the set of discriminations calculated for each chamber in parallel and for each type of plant.*

| Plants | $^{18}\varepsilon_{dark\_respi}$ (‰) | | $^{18}\varepsilon_{photosynthesis}$ (‰) | |
|---|---|---|---|---|
| | IRMS | OF-CEAS | IRMS | OF-CEAS |
| Fescue + soil | -16.9 ± 2.6 | | 5.0 ± 2.4 | |
| Banana tree + soil | -19.2 ± 2.2 | | 10.4 ± 3.6 | |
| Laurel + soil | -21.4 ± 5.8 | | 13.3 ± 3.3 | |
| Cypress + soil | -17.6 ± 0.6 | | X | |
| Maize + soil | -17.8 ± 0.9 | -15.9 ± 1.4 | 3.2 ± 2.6 | 6.2 ± 3.3 |
| Maize hydroponic | -16.7 ± 1.5 | -18.9 ± 4.7 | 7.7 ± 3.3 | 6.1 ± 3.8 |
| Fescue 2 + soil | -18.9 ± 0.6 | -19.0 ± 1.9 | 4.3 ± 1.2 | 4.7 ± 2.8 |
| Fescue 3 hydroponic | X* | -22.1 ± 7.4 | X* | 8.4 ± 3.1 |
| Soil only | -15.4 ± 1.1 | -17.8 ± 0.8 | | |

The overall $^{18}\varepsilon_{dark\_respi}$ values (Table 5) range from around - 16 to - 21 ‰ for [plant + soil] experiment. For hydroponic experiments the isotopic discriminations of respiration are in general higher than when plants are grown on soil. There is no significant difference on respiration discrimination between C3 and C4 plants (fescue and maize). For each plant, a positive discrimination exists for photosynthesis, which is between 3 and 10 ‰ with an extreme value at 13 ‰ which is not very reliable since it was determined in conditions of very small $O_2$ fluxes (see Fig.A1). It should also be noted that measurement uncertainty is higher when measurements have been made using the OF-CEAS technique rather than

612 the IRMS, but this does not prevent us from being able to interpret the data (Table 5). All
613 the data from these experiments are presented in the supplement (Fig.A1 and A2).

614

615 ## 4.2. GPP-$O_2$ quantification from model outputs

616

617 To infer past changes in the ratio of terrestrial to oceanic productivity, we give here the
618 GPP-$O_2$ of ocean and land calculated by three models used for PMIP exercises: MIROC-
619 ES2L, IPSL-CM5A-LR and MIROC-ESM for the pre-industrial period (PI), 6 ka BP period
620 and LGM period (Table 6).

621

| | Model | Domain | PI GPP-$O_2$ (Pmol $O_2$/yr) | MH (6 ka BP) GPP-$O_2$ (Pmol $O_2$/yr) | LGM GPP-$O_2$ (Pmol $O_2$/yr) |
|---|---|---|---|---|---|
| PMIP4-CMIP6 | MIROC-ES2L | Ocean | 0.67 | 0.67 | 0.68 |
| | | Land | 2.42 | 2.31 | 1.66 |
| PMIP3-CMIP5 | IPSL-CM5A-LR | Ocean | 0.79 | 0.81 | 0.70 |
| | | Land | 2.68 | 2.70 | 1.36 |
| | MIROC-ESM | Ocean | 0.66 | 0.69 | 0.66 |
| | | Land | 3.30 | 3.50 | 2.35 |

622 *Table 6. Output results from the MIROC-ES2L, IPSL-CM5A-LR and MIROC-ESM terrestrial and oceanic GPP-$O_2$ (Pmol $O_2$/yr)*
623 *models during the pre-industrial period (PI), during the mid-Holocene (MH, 6 ka BP) and during the LGM (last glacial*
624 *maximum).*

625

626 We can see for all model outputs that the terrestrial GPP-$O_2$ is always at least three times
627 greater than the oceanic GPP-$O_2$ for each time period. We also note that oceanic GPP-$O_2$
628 does not vary much over time. However, terrestrial GPP-$O_2$ is twice as high at pre-

industrial period and 6 ka BP than at LGM (2.4 and 1.7 Pmol $O_2$/yr respectively for MIROC-ES2L model).

# 5. Discussion

## 5.1. Interpretation of the respiratory and photosynthesis discriminations observed on the diversity of plants and experiments

### *5.1.1. Comparison between different types of plants*

Although there are differences in values between terrestrial photosynthetic fractionations, all plants studied here show terrestrial photosynthetic discrimination as in Paul et al. (2023). This is opposite to the classical use of a ${}^{18}\varepsilon_{photosynthesis}$ of 0 ‰ for terrestrial plants (Guy et al., 1993; Helman et al., 2005).

For all species grown on soil (fescue, banana tree, laurel, maize and cypress) the respiratory discriminations agree with results from the literature: - 17 ‰ in Paul et al. (2023) for fescue grown on soil and - 17 to - 19 ‰ in Guy et al. (1993) on a diversity of terrestrial plants. C3 and C4 plants cannot be distinguished in terms of respiratory discrimination.

Finally, the terrestrial respiratory discriminations for banana tree and laurel show the largest values. One hypothesis is that these organisms have thicker leaf tissue (sclerenchyma), in which diffusion is stronger, thus increasing the discrimination value. Particular attention should be paid to the fact that the uncertainty of these measurements is quite high.

### *5.1.2. Comparison between plants/soil and hydroponics experiments*

Hydroponics experiments allows study of the plant respiration without influence of the soil respiration. We observe that respiratory isotopic fractionation is greater in experiments with plants alone than those including soil respiration. We can conclude from this observation that plant dark respiration fractionates more than soil respiration. This result is supported by our determination of $^{18}\varepsilon_{soil\_respi}$ which is less negative (- 15.4 ‰) than the $^{18}\varepsilon_{plant\_respi}$ values (between - 16 ‰ and - 19 ‰). Our results agree with previous studies which found relatively small discrimination values for soil respiration because of diffusion (Angert et al., 2001)

## 5.2. The existence of the terrestrial photosynthesis fractionation

When we calculated the value for $^{18}\varepsilon_{\mathrm{photosynthesis}}$ in Table 5, we found a positive discrimination value for each species studied. The calculation of $^{18}\varepsilon_{photosynthesis}$ depends on the flux of dioxygen uptake, the value for $^{18}\varepsilon_{\mathrm{respiration}}$ during the day and the value for $\delta^{18}O_{lw}$. We thus evaluate how uncertainties on these determinations affect our results. We first calculate a net photosynthetic discrimination making the extreme hypothesis that no dioxygen uptake occurs in parallel to the photosynthesis. With this extreme assumption, we obtain discrimination values which are at best 1 ‰ lower than the values shown in Table 5. An error in the estimate of the $O_2$ consumption flux during the day can hence not explain the positive value for $^{18}\varepsilon_{photosynthesis}$. A second source of uncertainty is the value of the discrimination associated with oxygen uptake. For example, for the fescue experiment, with a fairly low $^{18}\varepsilon_{photosynthesis}$ value, a discrimination for terrestrial respiration of at least - 40 ‰ should be imposed so that the calculated $^{18}\varepsilon_{photosynthesis}$ is equal to zero (Table A1). This value is unrealistic with respect to the values for

680 $^{18}\varepsilon_{\mathrm{respiration}}$determined in the previous section or in any previous studies. The last source
681 of uncertainty is the determination of the $\delta^{18}O_{lw}$. With a $\delta^{18}O_{lw}$ value larger than the one
682 measured here, we would have determined a lower $^{18}\varepsilon_{photosynthesis}$. Our determination of
683 $\delta^{18}O_{lw}$ is, however, likely already overestimated. Indeed, $\delta^{18}O_{lw}$ was measured only at the
684 end of the experiment, while we observed that $\delta^{18}O_{lw}$ tends to increase progressively
685 during the course of the experiment, by up to 2 ‰ (Paul et al., 2023). This means that the
686 $\delta^{18}O_{lw}$ value we used in the calculation is potentially higher than the average value actually
687 experienced by the plants during photosynthesis. If $\delta^{18}O_{lw}$ is already overestimated,
688 further increasing it from 5 ‰ to 9 ‰ to force $^{18}\varepsilon_{photosynthesis}$ to zero would be
689 inconsistent with the experimental evidence. Therefore, the discrepancy cannot be
690 explained by uncertainty on the $\delta^{18}O_{lw}$ determination, which supports the conclusion that
691 $^{18}\varepsilon_{photosynthesis}$ remains positive under these biological chamber conditions (Table A2).
692
693
694 We thus conclude that in biological chambers experiments, which is the closest analog
695 for real conditions in this type of experiment, $^{18}\varepsilon_{\mathrm{photosynthesis}}$ is positive. This observation
696 still remains difficult to explain.

697 Water oxidation in photosystem II is not expected to introduce any isotopic discrimination
698 (Tcherkez and Farquhar, 2007). Involving preferential diffusion of the light isotopologues
699 in the stomates (either preferential diffusion of $H_2{}^{16}O$ vs $H_2{}^{18}O$ in the leaf water before
700 photosynthesis or preferential diffusion of $^{16}O^{16}O$ vs $^{16}O^{18}O$ of produced $O_2$ after
701 photosynthesis) would also go into the wrong direction. These diffusion effects would
702 indeed lead to a lower difference between $\delta^{18}O_{lw}$ and $\delta^{18}O$ of $O_2$ in the atmosphere of the
703 biological chamber than the true difference and hence better lead to an underestimated
704 value of our calculated $^{18}\varepsilon_{photosynthesis}$. The last possible hypothesis would be that an
705 additional oxygen consuming process occurs during photosynthesis (Eisenstadt et al.,
706 2010). This process should be associated with a strong negative discrimination to

compensate for the calculated $^{18}\varepsilon_{photosynthesis}$. Summarizing, we cannot yet explain why $^{18}\varepsilon_{photosynthesis}$ is associated with a positive isotopic discrimination. However, coherent observations for several biological chambers experiments and several plants suggest that this discrimination is true and should be considered when calculating a global budget for the Dole effect.

## 5.3. Implications of these fractionation factors for interpreting the global Dole effect

We use here the latest estimates of the different fractionation factors and global estimates of terrestrial and oceanic productivities during the last deglaciation to reevaluate the main drivers of the Dole effect. In particular, we aim at quantifying the role of the ratio of terrestrial to oceanic productivity as the main drivers of the Dole effect variations in the past.

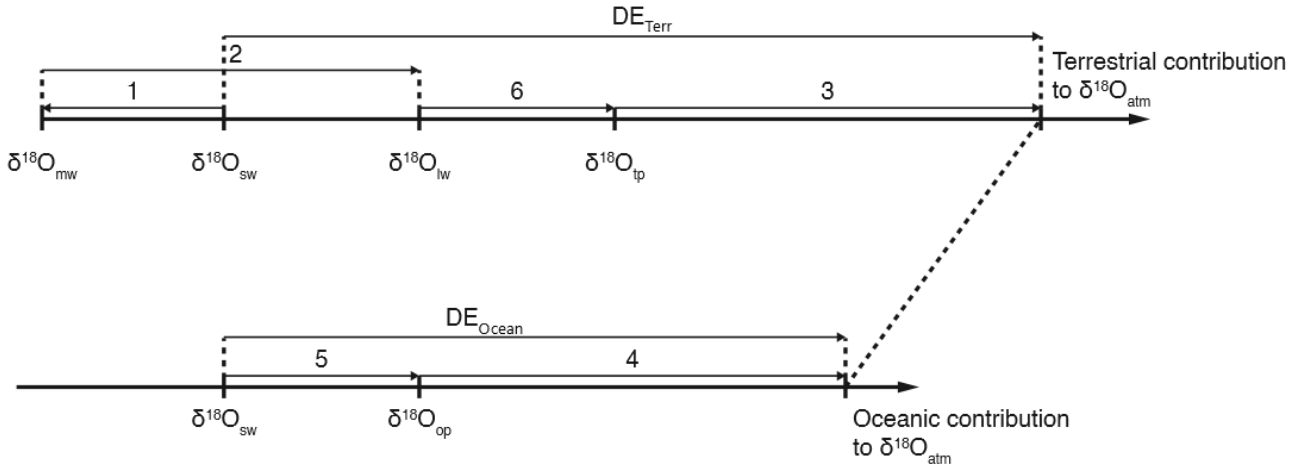


*Figure 5. Diagram of the main contributions to $\delta^{18}O_{atm}$. (1) Fractionation of water associated with evaporation and precipitation. (2) Fractionation of water associated with evapotranspiration. (3) Fractionation of atmospheric oxygen during*

*terrestrial respiration. (4) Fractionation of atmospheric oxygen during oceanic respiration. (5) Fractionation associated with oceanic photosynthesis. (6) Fractionation during terrestrial photosynthesis. $DE_{Terr}$ = terrestrial Dole effect and $DE_{Oceanic}$ = oceanic Dole effect (modified from Landais et al., 2007).*

For an updated calculation of the Dole effect, we rely as much as possible on the latest available estimates for isotopic discriminations during biological processes. Our study is focused on the terrestrial plants so that we only modified the terrestrial Dole effect compared to previous studies. We use a $^{18}\varepsilon_{photosynthesis}$ value of 3.7 ‰ as given by Paul et al. (2023). This is significantly larger than the 0 ‰ value usually considered but still at the lowest end of the estimates found in the present study. As a sensitivity test, we also present in the Table A3 an estimate performed with the most extreme (and irrealistic) value $^{18}\varepsilon_{photosynthesis}$ = 13.3‰. For $^{18}\varepsilon_{dark\_respi}$, we use a global value of 17 ‰ in agreement with Paul et al. (2023) and the present study, which is slightly lower than the latest estimate of 17.7 ‰ given by Luz and Barkan (2011). Sensitivity tests were also performed in Table A3 with $^{18}\varepsilon_{dark\_respi}$ ranging from 16 to 21 ‰ as found in the different biological experiments above. With these new estimates, we calculate a terrestrial effect of 26.5 ‰ (24.7 to 32.9 ‰ when adding the large uncertainties on $^{18}\varepsilon_{photosynthesis}$ and $^{18}\varepsilon_{dark\_respi}$), a value which is larger than the previous determination (23.5 ‰) from Luz and Barkan (2011). The main difference between the two estimates is mostly due to our positive value for $^{18}\varepsilon_{photosynthesis}$. We kept the latest value for oceanic Dole effect (23.5 ‰) as given by Luz and Barkan (2011). Our new Dole effect estimate is presented in Table 7 to be compared to the previous estimates displayed in Table 1.

*Table 7. Parameters used to calculate oceanic, terrestrial and the current and LGM global Dole effects in our study. * stands for parameters determined in our study; [1]West et al. (2008) and Benson and Krause (1984); [2]Landais et al. (2007); [3]Luz and Barkan (2011).*

| | PI | LGM |
|---|---|---|
| $\delta^{18}O_{lw}$ | 5.7[1] | 6.7[1] |
| ${}^{18}\varepsilon_{respiration\_terr}$ | 17* | 16.9[2] |
| ${}^{18}\varepsilon_{photosynthesis\_terr}$ | 3.7* | 3.7* |
| $DE_{ocean}$ | 23.5[3] | 23.5[3] |
| $DE_{terr}$ | 26.4 | 26.3 |

To address the change of the Dole effect over the last deglaciation, we estimate Dole effect for the last glacial maximum. In line with previous studies, we assume that the isotopic discrimination for the different biological processes does not vary with time. However, because of the global change in $\delta^{18}O_{sw}$ and changes in the atmospheric hydrological cycle, $\delta^{18}O_{lw}$ varies during this period. This is also the case for ${}^{18}\varepsilon_{soil\_respi}$ because of the latitudinal changes of the repartition of vegetation and for the ratio between C3 and C4 plants because of $CO_2$ concentration change in the atmosphere. The change in the proportion of C3 and C4 plants affects the value for global ${}^{18}\varepsilon_{respiration}$ due to its influence on the proportion of photorespiration in the global $O_2$ uptake (Landais et al., 2007).

First, $\delta^{18}O_{lw}$ has been calculated to be higher during the LGM by 1 ‰ compared to the pre-industrial period (Landais et al., 2007; Ciais et al., 2012). The change in ${}^{18}\varepsilon_{soil\_respi}$ was calculated by Landais et al. (2007); it is 0.5 ‰ stronger during the LGM than today, resulting in a variation of less than 0.3 ‰ for the global ${}^{18}\varepsilon_{respiration}$ when considering the fraction of soil respiration on the total respiration. Finally, the change in the proportion GPP-$O_2$ associated with C3 and C4 plants is calculated from the outputs of the models

767 presented in Section 3.3 and by applying the calculation described above for $O_2$
768 consumption via photorespiration by C3 plants. It results in a variation of about 0.1 ‰ on

769 the global ${}^{18}\varepsilon_{respiration}$. The global $\delta^{18}O_{sw}$ value is higher by 1 ‰ during the LGM
770 compared to the recent period which cancels the 1 ‰ increase in global $\delta^{18}O_{lw}$ during
771 LGM when calculating the terrestrial Dole effect. We thus estimate that the terrestrial DE
772 is lower by 0.1 ‰ during the LGM compared to today. We take the same value for the
773 oceanic Dole effect at LGM than at present.

774

| | PI | MH (6 ka BP) | LGM | 775 |
|---|---|---|---|---|
| IPSL-CM5A-LR | 25.5 | 25.5 | 25.1 | 776 |
| MIROC-ES2L | 25.5 | 25.5 | 25.2 | 777 |
| MIROC-ESM | 25.7 | 25.7 | 25.4 | 778 |

779 *Table 8. Global Dole effects based on GPP-$O_2$ variations of three model outputs (MIROC-ES2L, IPSL-CM5A-LR and MIROC-*
780 *ESM) using our estimates of the terrestrial and oceanic Dole effect for different periods (pre-industrial period (PI), mid-*
781 *holocene (MH, 6 ka BP) and LGM). For the 6 ka BP, we assumed that the terrestrial and oceanic Dole effects are the same*
782 *as for the PI, only the GPP-$O_2$ are different.*

783 In order to calculate the global Dole effect from the estimates of the terrestrial and
784 oceanic contributions displayed in Table 8, we use the GPP-$O_2$ determination performed
785 with PMIP model outputs presented in section 4.2. Because we have 3 different models,
786 we end up with 3 different estimates of the global Dole effect for each period.

787 Our determinations for the pre-industrial Dole effect are higher (average value of 25.5 ‰,
788 Table 8; sensitivity tests lead to variations between 24.7 and 32.9‰, Table A3) than the
789 measured values (24 ‰) by 1.5 ‰. We also find that the difference between the Dole
790 effect at LGM and at PI (*e.g.* with the IPSL-CM5A-LR model) is 0.4 ‰. This difference
791 cannot be reconciled with the data showing a difference of 0 ± 0.1 ‰ (Fig. 4). Such data-

792 model mismatch can be due to a change in the fractionation factors for respiration and
793 photosynthesis between the LGM and today hence motivating the studies of the effects
794 of the climatic conditions on the fractionation factors.

795 We also did an attempt to calculate the 6 ka Dole effect with our updated estimate of
796 terrestrial Dole effect. If we keep the same values for terrestrial and oceanic Dole effect
797 than at PI, we do not calculate any change in the global Dole effect ($DE_{PI} - DE_{6ka}$ = 0 ‰
798 for all studies with all models, Table 8) while there is a significative change of - 0.4 ‰ in
799 the measured Dole effect (Fig. 4). To reproduce the - 0.4 ‰ variation in the global Dole
800 effect at 6 ka in our study, the value of oceanic GPP-$O_2$ would have to double compared
801 with what is given by the various models presented and field observations. We can
802 therefore conclude that it is impossible to explain the change in the Dole effect at 6 ka by
803 a change in the ratio of terrestrial vs oceanic gross primary productivity (Eq. 6). This argues
804 that the oceanic or terrestrial Dole effects vary with time and that the DE variations
805 observed in ice cores (Fig. 4) cannot be explained only by fluctuations in the relative
806 proportions of oceanic and terrestrial gross primary productivity as suggested by Bender
807 et al. (1994) and by Ciais et al. (2012). This finding confirms previous studies (Landais et
808 al., 2007; Luz and Barkan, 2011; Severinghaus et al., 2009; Seltzer et al., 2017; Huang et al.,
809 2020) suggesting that variations in the Dole effect are influenced by low latitude changes
810 in atmospheric hydrological cycle leading to changes in $\delta^{18}O$ of the meteoric water
811 transmitted to $\delta^{18}O$ of soil water, to $\delta^{18}O_{lw}$ and to $\delta^{18}O_{atm}$ through photosynthesis. In
812 addition, Severinghaus et al. (2009) proposed that changes in tropical soil respiration,
813 associated with weaker isotopic fractionation, could also have played a key role in driving
814 the observed Dole effect variations. Together, these processes would well explain the 6ka
815 minimum in DE which is also captured in the $\delta^{18}O_{calcite}$ of low latitude speleothem, also
816 sensitive to variations in the $\delta^{18}O$ of meteoric water (Hu et al., 2019).

817

# 6. Conclusion

Using closed chamber experiments as an analogue of the terrestrial biosphere, we have confirmed a previous study that there is a positive $^{18}O$ discrimination (between 3 and 8 ‰) during photosynthesis for all plants studied. The values found for the $^{18}O$ discrimination during respiration of different plants (- 16 to - 21‰) agree with the previous published studies. Using these new values as well as outputs from PMIP models for the GPP-$O_2$, the global Dole effect has been reevaluated. An average value of 25.5‰ is found for the present-day which is significantly too high compared to the estimate of 24 ‰ hence questioning the applicability of the fractionation coefficients found for some species to a global calculation. Moreover, when we look at the change of the calculated Dole effect between the LGM and the PI, we do find some significant change which is not in agreement with the data. This suggest that fractionation factors for the biological processes vary with time, probably because of a change in the climatic conditions, a hypothesis already proposed by Stolper et al. (2018).

In this study, we made several hypotheses which should be explored in the future. First, we assumed, as in previous studies, that the fractionations associated with biological processes do not vary with time nor with climatic conditions Second, in our study, we did not reevaluate with a similar approach the oceanic biological fractionations. In the future, it is thus important to reevaluate the terrestrial and oceanic fractionation factors for a variety of species in different environmental and climatic conditions using a set-up similar to the one used here which is intermediate between the lab experiments at the cell scale and the measurements on field with no control on environmental conditions and their history.

## Author contributions

AL, CPi and CPa designed the project. CPi, JS, SD and CPa carried out experiments at ECOTRON of Montpellier and CPa, FP, RJ, AD and OJ at LSCE. CPi, DR and CPa carried out maintenance and characterized the optical spectrometer. CPa, CPi and AL analyzed the data from the optical spectrometer and CPa and AL analysed the data from IRMS. CPa, Al and CPi prepared the manuscript with contributions from AM.

## Acknowledgements

The research leading to these results has received funding from the European Research Council under the European Union H2020 Programme (H2020/20192024)/ERC grant agreement no. 817493 (ERC ICORDA) and ANR HUMI17. The authors acknowledge the scientific and technical support of PANOPLY (Plateforme ANalytique géOsciences Paris-sacLaY), Paris-Saclay University, France. Our thanks also to go to AQUA-OXY (CNRS IIT project). This study benefited from the CNRS resources allocated to the French ECOTRONS Research Infrastructure, from the Occitanie Region and FEDER investments as well as from the state allocation 'Investissement d'Avenir' AnaEE- France ANR-11-INBS-0001. We would also like to thank Abdelaziz Faez and Olivier Ravel from ECOTRON of Montpellier for their help and Emeritus Prof. Phil Ineson from University of York.

## References

Aggarwal, P. K., Alduchov, O. A., Froehlich, K. O., Araguas-Araguas, L. J., Sturchio, N. C., and Kurita, N.: Stable isotopes in global precipitation: A unified interpretation based on atmospheric moisture residence time, Geophysical Research Letters, 39, 2012GL051937, https://doi.org/10.1029/2012GL051937, 2012.

Anderson, W. T., Bernasconi, S. M., McKenzie, J. A., Saurer, M., and Schweingruber, F.: Model evaluation for reconstructing the oxygen isotopic composition in precipitation from tree ring cellulose over the last century, Chemical Geology, 182, 121–137, https://doi.org/10.1016/S0009-2541(01)00285-6, 2002.

Angert, A. and Luz, B.: Fractionation of oxygen isotopes by root respiration: Implications for the isotopic composition of atmospheric O2, Geochimica et Cosmochimica Acta, 65, 1695–1701, https://doi.org/10.1016/S0016-7037(01)00567-1, 2001.

Angert, A., Luz, B., and Yakir, D.: Fractionation of oxygen isotopes by respiration and diffusion in soils and its implications for the isotopic composition of atmospheric $O_2$, Global Biogeochemical Cycles, 15, 871–880, https://doi.org/10.1029/2000GB001371, 2001.

Angert, A., Barkan, E., Barnett, B., Brugnoli, E., Davidson, E. A., Fessenden, J., Maneepong, S., Panapitukkul, N., Randerson, J. T., Savage, K., Yakir, D., and Luz, B.: Contribution of soil respiration in tropical, temperate, and boreal forests to the $^{18}O$ enrichment of atmospheric $O_2$, *Global Biogeochem. Cy.*, 17, 1089, https://doi.org/10.1029/2003GB002056, 2003.

Barkan, E. and Luz, B.: High precision measurements of 17 O/ 16 O and 18 O/ 16 O ratios in H 2 O, Rapid Comm Mass Spectrometry, 19, 3737–3742, https://doi.org/10.1002/rcm.2250, 2005.

Bazin, L., Landais, A., Lemieux-Dudon, B., Toyé Mahamadou Kele, H., Veres, D., Parrenin, F., Martinerie, P., Ritz, C., Capron, E., Lipenkov, V., Loutre, M.-F., Raynaud, D., Vinther, B., Svensson, A., Rasmussen, S. O., Severi, M., Blunier, T., Leuenberger, M., Fischer, H., Masson-

Delmotte, V., Chappellaz, J., and Wolff, E.: An optimized multi-proxy, multi-site Antarctic ice and gas orbital chronology (AICC2012): 120–800 ka, Clim. Past, 9, 1715–1731, https://doi.org/10.5194/cp-9-1715-2013, 2013.

Bender, M., Sowers, T., Dickson, M.-L., Orchardo, J., Grootes, P., Mayewski, P. A., and Meese, D. A.: Climate correlations between Greenland and Antarctica during the past 100,000 years, Nature, 372, 663–666, https://doi.org/10.1038/372663a0, 1994.

Bender, M. L.: The δ 18 O of dissolved O 2 in seawater: A unique tracer of circulation and respiration in the deep sea, J. Geophys. Res., 95, 22243–22252, https://doi.org/10.1029/JC095iC12p22243, 1990.

Benson, B. B., and Krause, D.: The concentration and isotopic fractionation of oxygen dissolved in fresh water and seawater in equilibrium with the atmosphere, Limnol. Oceanogr., 29, 620–632, https://doi.org/10.4319/lo.1984.29.3.0620

Bintanja, R., van de Wal, R. S. W., and Oerlemans, J.: Modelled atmospheric temperatures and global sea levels over the past million years, *Nature*, 437, 125–128, https://doi.org/10.1038/nature03975, 2005.

Blunier, T., Barnett, B., Bender, M. L., and Hendricks, M. B.: Biological oxygen productivity during the last 60,000 years from triple oxygen isotope measurements, Global Biogeochemical Cycles, 16, https://doi.org/10.1029/2001GB001460, 2002.

Bouchet, M., Landais, A., Grisart, A., Parrenin, F., Prié, F., Jacob, R., Fourré, E., Capron, E., Raynaud, D., Lipenkov, V. Y., Loutre, M.-F., Extier, T., Svensson, A., Legrain, E., Martinerie, P., Leuenberger, M., Jiang, W., Ritterbusch, F., Lu, Z.-T., and Yang, G.-M.: The AICC2023 chronological framework and associated timescale for the EPICA Dome C ice core, Ice Dynamics/Ice Cores/Milankovitch, https://doi.org/10.5194/egusphere-2023-1081, 2023.

Cernusak, L. A., Barbour, M. M., Arndt, S. K., Cheesman, A. W., English, N. B., Feild, T. S., Helliker, B. R., Holloway-Phillips, M. M., Holtum, J. A. M., Kahmen, A., McInerney, F. A.,

Duplessy, J.-C., Labeyrie, L., and Waelbroeck, C.: Constraints on the ocean oxygen isotopic enrichment between the Last Glacial Maximum and the Holocene: Paleoceanographic implications, *Quat. Sci. Rev.*, 21, 315–330, https://doi.org/10.1016/S0277-3791(01)00107-X, 2002.

Munksgaard, N. C., Simonin, K. A., Song, X., Stuart-Williams, H., West, J. B., and Farquhar, G. D.: Stable isotopes in leaf water of terrestrial plants, Plant Cell & Environment, 39, 1087–1102, https://doi.org/10.1111/pce.12703, 2016.

Cheng, H., Edwards, R. L., Sinha, A., Spötl, C., Yi, L., Chen, S., Kelly, M., Kathayat, G., Wang, X., Li, X., Kong, X., Wang, Y., Ning, Y., and Zhang, H.: The Asian monsoon over the past 640,000 years and ice age terminations, Nature, 534, 640–646, https://doi.org/10.1038/nature18591, 2016.

Ciais, P., Tagliabue, A., Cuntz, M., Bopp, L., Scholze, M., Hoffmann, G., Lourantou, A., Harrison, S. P., Prentice, I. C., Kelley, D. I., Koven, C., and Piao, S. L.: Large inert carbon pool in the terrestrial biosphere during the Last Glacial Maximum, Nature Geosci, 5, 74–79, https://doi.org/10.1038/ngeo1324, 2012.

Dole, M.: The relative atomic weight of oxygen in water and in air, *J. Am. Chem. Soc.*, 57, 2731–2733, https://doi.org/10.1021/ja01315a511, 1935.

Dreyfus, G. B., Parrenin, F., Lemieux-Dudon, B., Durand, G., Masson-Delmotte, V., Jouzel, J., Barnola, J.-M., Panno, L., Spahni, R., Tisserand, A., Siegenthaler, U., and Leuenberger, M.: Anomalous flow below 2700 m in the EPICA Dome C ice core detected using δ 18 O of atmospheric oxygen measurements, Clim. Past, 3, 341–353, https://doi.org/10.5194/cp-3-341-2007, 2007.

Eisenstadt, D., Barkan, E., Luz, B., and Kaplan, A.: Enrichment of oxygen heavy isotopes during photosynthesis in phytoplankton, Photosynth Res, 103, 97–103, https://doi.org/10.1007/s11120-009-9518-z, 2010.

943 Extier, T., Landais, A., Bréant, C., Prié, F., Bazin, L., Dreyfus, G., Roche, D. M., and
944 Leuenberger, M.: On the use of $\delta^{18}O_{atm}$ for ice core dating, Quat. Sci. Rev., 185, 244-257,
945 https://doi.org/10.1016/j.quascirev.2018.02.008, 2018.

946 Farquhar, G. D., Lloyd, J., Taylor, J. A., Flanagan, L. B., Syvertsen, J. P., Hubick, K. T., Wong,
947 S. C., and Ehleringer, J. R.: Vegetation effects on the isotope composition of oxygen in
948 atmospheric CO2, Nature, 363, 439–443, https://doi.org/10.1038/363439a0, 1993.

949 Flanagan, L. B., Bain, J. F., and Ehleringer, J. R.: Stable oxygen and hydrogen isotope
950 composition of leaf water in C3 and C4 plant species under field conditions, Oecologia,
951 88, 394–400, https://doi.org/10.1007/BF00317584, 1991.

952 Gillon, J. and Yakir, D.: Influence of Carbonic Anhydrase Activity in Terrestrial Vegetation
953 on the 18 O Content of Atmospheric CO2, Science, 291, 2584–2587,
954 https://doi.org/10.1126/science.1056374, 2001.

955 Guy, R. D., Berry, J. A., Fogel, M. L., and Hoering, T. C.: Differential fractionation of oxygen
956 isotopes by cyanide-resistant and cyanide-sensitive respiration in plants, Planta, 177, 483–
957 491, https://doi.org/10.1007/BF00392616, 1989.

958 Guy, R. D., Berry, J. A., Fogel, M. L., Turpin, D. H., and Weger, H. G.: Fractionation of the
959 stable isotopes of oxygen during respiration by plants: The basis of a new technique to
960 estimate partitioning to the alternative path, Plant Respiration., Molecular, Biochemical
961 and Physiological Aspects, SPB Academic Publishing, The Hague, the Netherlands, 443–
962 453, 1992.

963 Guy, R. D., Fogel, M. L., and Berry, J. A.: Photosynthetic Fractionation of the Stable Isotopes
964 of Oxygen and Carbon, Plant Physiol., 101, 37–47, https://doi.org/10.1104/pp.101.1.37,
965 1993.

966 Helliker, B. R. and Richter, S. L.: Subtropical to boreal convergence of tree-leaf
967 temperatures, Nature, 454, 511–514, https://doi.org/10.1038/nature07031, 2008.

968 Helman, Y., Barkan, E., Eisenstadt, D., Luz, B., and Kaplan, A.: Fractionation of the Three
969 Stable Oxygen Isotopes by Oxygen-Producing and Oxygen-Consuming Reactions in
970 Photosynthetic Organisms, Plant Physiology, 138, 2292–2298,
971 https://doi.org/10.1104/pp.105.063768, 2005.

972 Hendricks, M. B., Bender, M. L., and Barnett, B. A.: Net and gross O2 production in the
973 southern ocean from measurements of biological O2 saturation and its triple isotope
974 composition, Deep Sea Research Part I: Oceanographic Research Papers, 51, 1541–1561,
975 https://doi.org/10.1016/j.dsr.2004.06.006, 2004.

976 Hoffmann, G., Cuntz, M., Weber, C., Ciais, P., Friedlingstein, P., Heimann, M., Jouzel, J.,
977 Kaduk, J., Maier-Reimer, E., Seibt, U., and Six, K.: A model of the Earth's Dole effect, Global
978 Biogeochemical Cycles, 18, 2003GB002059, https://doi.org/10.1029/2003GB002059,
979 2004.

980 Hu, Y. B., Xiao, W., Qian, Y. F., Liu, Q., Xie, C. Y., Zhang, X. F., Zhang, W. Q., Liu, S. D., and
981 Lee, X. H.: [Effects of Water Vapor Source and Local Evaporation on the Stable Hydrogen
982 and Oxygen Isotopic Compositions of Precipitation]., Huanjing kexue, 40, 573–581,
983 https://doi.org/10.13227/j.hjkx.201805227, 2019.

984 Huang, E., Wang, P., Wang, Y., Yan, M., Tian, J., Li, S., and Ma, W.: Dole effect as a
985 measurement of the low-latitude hydrological cycle over the past 800 ka, Sci. Adv., 6,
986 eaba4823, https://doi.org/10.1126/sciadv.aba4823, 2020.

987 Keeling, R. F.: Development of an interferometric oxygen analyzer for precise
988 measurement of the atmospheric O2 mole fraction, Harvard Univ., Cambridge, Mass.,
989 1988.

990 Keeling, R. F. and Shertz, S. R.: Seasonal and interannual variations in atmospheric oxygen
991 and implications for the global carbon cycle, Nature, 358, 723–727,
992 https://doi.org/10.1038/358723a0, 1992.

Kiddon, J., Bender, M. L., Orchardo, J., Caron, D. A., Goldman, J. C., and Dennett, M.: Isotopic fractionation of oxygen by respiring marine organisms, Global Biogeochemical Cycles, 7, 679–694, https://doi.org/10.1029/93GB01444, 1993.

Kim, Y., and Kang, D.-J.: Oxygen isotopic fractionation during dissolved oxygen consumption in the bottom layer of the Ulleung Basin, East/Japan Sea, *Front. Mar. Sci.*, 10, 1276028, https://doi.org/10.3389/fmars.2023.1276028, 2024.

Kroopnick, P. and Craig, H.: Atmospheric Oxygen: Isotopic Composition and Solubility Fractionation, Science, 175, 54–55, https://doi.org/10.1126/science.175.4017.54, 1972.

Laisk, A. and Edwards, G. E.: Oxygen and electron flow in C 4 photosynthesis: Mehler reaction, photorespiration and CO 2 concentration in the bundle sheath, Planta, 205, 632–645, https://doi.org/10.1007/s004250050366, 1998.

Landais, A., Barkan, E., Yakir, D., and Luz, B.: The triple isotopic composition of oxygen in leaf water, Geochimica et Cosmochimica Acta, 70, 4105–4115, https://doi.org/10.1016/j.gca.2006.06.1545, 2006.

Landais, A., Lathiere, J., Barkan, E., and Luz, B.: Reconsidering the change in global biosphere productivity between the Last Glacial Maximum and present day from the triple oxygen isotopic composition of air trapped in ice cores, Global Biogeochemical Cycles, 21, 2006GB002739, https://doi.org/10.1029/2006GB002739, 2007.

Landais, A., Dreyfus, G., Capron, E., Masson-Delmotte, V., Sanchez-Goñi, M. F., Desprat, S., Hoffmann, G., Jouzel, J., Leuenberger, M., and Johnsen, S.: What drives the millennial and orbital variations of δ18Oatm?, Quaternary Science Reviews, 29, 235–246, https://doi.org/10.1016/j.quascirev.2009.07.005, 2010.

Lisiecki, L. E. and Raymo, M. E.: A Pliocene-Pleistocene stack of 57 globally distributed benthic δ 18 O records, Paleoceanography, 20, 2004PA001071, https://doi.org/10.1029/2004PA001071, 2005.

1018 Lisiecki, L. E. and Stern, J. V.: Regional and global benthic δ 18 O stacks for the last glacial
1019 cycle: Last Glacial Cycle Benthic δ 18 O, Paleoceanography, 31, 1368–1394,
1020 https://doi.org/10.1002/2016PA003002, 2016.

1021 Liu, H., Zartman, R. E., Ireland, T. R., and Sun, W.: Global atmospheric oxygen variations
1022 recorded by Th/U systematics of igneous rocks, Proc. Natl. Acad. Sci. U.S.A., 116, 18854–
1023 18859, https://doi.org/10.1073/pnas.1902833116, 2019.

1024 Luz, B. and Barkan, E.: The isotopic composition of atmospheric oxygen: ISOTOPIC
1025 COMPOSITION OF AIR OXYGEN, Global Biogeochem. Cycles, 25, n/a-n/a,
1026 https://doi.org/10.1029/2010GB003883, 2011.

1027 Luz, B., Barkan, E., Bender, M. L., Thiemens, M. H., and Boering, K. A.: Triple-isotope
1028 composition of atmospheric oxygen as a tracer of biosphere productivity, Nature, 400,
1029 547–550, https://doi.org/10.1038/22987, 1999.

1030 Malaizé, B., Paillard, D., Jouzel, J., and Raynaud, D.: The Dole effect over the last two glacial-
1031 interglacial cycles, J. Geophys. Res., 104, 14199–14208,
1032 https://doi.org/10.1029/1999JD900116, 1999.

1033 Marra, J.: Approaches to the Measurement of Plankton Production, in: Phytoplankton
1034 Productivity, edited by: Williams, P. J. L. B., Thomas, D. N., and Reynolds, C. S., Wiley, 78–
1035 108, https://doi.org/10.1002/9780470995204.ch4, 2002.

1036 Milcu, A., Allan, E., Roscher, C., Jenkins, T., Meyer, S. T., Flynn, D., Bessler, H., Buscot, F.,
1037 Engels, C., Gubsch, M., König, S., Lipowsky, A., Loranger, J., Renker, C., Scherber, C., Schmid,
1038 B., Thébault, E., Wubet, T., Weisser, W. W., Scheu, S., and Eisenhauer, N.: Functionally and
1039 phylogenetically diverse plant communities key to soil biota, Ecology, 94, 1878–1885,
1040 https://doi.org/10.1890/12-1936.1, 2013.

1041 Paul, C., Piel, C., Sauze, J., Pasquier, N., Prie, F., Devidal, S., Jacob, R., Dapoigny, A., Jossoud,
1042 O., Milcu, A., and Landais., A: Determination of respiration and photosynthesis

fractionation factors for atmospheric dioxygen inferred from a vegetation-soil-atmosphere analogue of the terrestrial biosphere in closed chambers, BG, 20, 1047-1062, https://doi.org/10.5194/bg-20-1047-2023, 2023.

Paul, C., Piel, C., Sauze, J., Jossoud, O., Dapoigny, A., Romanini, D., Prié, F., Devidal, S., Jacob, R., Milcu, A., and Landais, A.: A multiplexing system for quantifying oxygen fractionation factors in closed chambers, *Geosci. Instrum. Method. Data Syst.*, 14, 91–102, https://doi.org/10.5194/gi-14-91-2025, 2025.

Paul, C., Piel, C., Sauze, J., Jossoud, O., Dapoigny, A., Romanini, D., Prie, F., Devidal, S., Jacob, R., Milcu, A., and Landais., A : A multiplexing system for quantifying oxygen fractionation factors in closed chambers, https://doi.org/10.5194/egusphere-2024-1755.

Pack, A., Höweling, A., Hezel, D. C., Stefanak, M. T., Beck, A.-K., Peters, S. T. M., Sengupta, S., Herwartz, D., and Folco, L.: Tracing the oxygen isotope composition of the upper Earth's atmosphere using cosmic spherules, Nat Commun, 8, 15702, https://doi.org/10.1038/ncomms15702, 2017.

Parrenin, F., Barnola, J.-M., Beer, J., Blunier, T., Castellano, E., Chappellaz, J., Dreyfus, G., Fischer, H., Fujita, S., Jouzel, J., Kawamura, K., Lemieux-Dudon, B., Loulergue, L., Masson-Delmotte, V., Narcisi, B., Petit, J.-R., Raisbeck, G., Raynaud, D., Ruth, U., Schwander, J., Severi, M., Spahni, R., Steffensen, J. P., Svensson, A., Udisti, R., Waelbroeck, C., and Wolff, E.: The EDC3 chronology for the EPICA Dome C ice core, Clim. Past, 3, 485–497, https://doi.org/10.5194/cp-3-485-2007, 2007.

Petit, J. R., Jouzel, J., Raynaud, D., Barkov, N. I., Barnola, J.-M., Basile, I., Bender, M., Chappellaz, J., Davis, M., Delaygue, G., Delmotte, M., Kotlyakov, V. M., Legrand, M., Lipenkov, V. Y., Lorius, C., PÉpin, L., Ritz, C., Saltzman, E., and Stievenard, M.: Climate and atmospheric history of the past 420,000 years from the Vostok ice core, Antarctica, Nature, 399, 429–436, https://doi.org/10.1038/20859, 1999.

1068 Prentice, I. C., Cleator, S. F., Huang, Y. H., Harrison, S. P., and Roulstone, I.: Reconstructing
1069 ice-age palaeoclimates: Quantifying low-CO2 effects on plants, Global and Planetary
1070 Change, 149, 166–176, https://doi.org/10.1016/j.gloplacha.2016.12.012, 2017.

1071 Schrag, D. P., Adkins, J. F., McIntyre, K., Alexander, J. L., Hodell, D. A., Charles, C. D., and
1072 McManus, J. F.: The oxygen isotopic composition of seawater during the Last Glacial
1073 Maximum, Quaternary Science Reviews, 21, 331–342, https://doi.org/10.1016/S0277-
1074 3791(01)00110-X, 2002.

1075 Seltzer, A. M., Severinghaus, J. P., Andraski, B. J., and Stonestrom, D. A.: Steady state
1076 fractionation of heavy noble gas isotopes in a deep unsaturated zone, Water Resources
1077 Research, 53, 2716–2732, https://doi.org/10.1002/2016WR019655, 2017.

1078 Severinghaus, J. P., Beaudette, R., Headly, M. A., Taylor, K., and Brook, E. J.: Oxygen-18 of
1079 O 2 Records the Impact of Abrupt Climate Change on the Terrestrial Biosphere, Science,
1080 324, 1431–1434, https://doi.org/10.1126/science.1169473, 2009.

1081 Sigl, M., Fudge, T. J., Winstrup, M., Cole-Dai, J., Ferris, D., McConnell, J. R., Taylor, K. C.,
1082 Welten, K. C., Woodruff, T. E., Adolphi, F., Bisiaux, M., Brook, E. J., Buizert, C., Caffee, M. W.,
1083 Dunbar, N. W., Edwards, R., Geng, L., Iverson, N., Koffman, B., Layman, L., Maselli, O. J.,
1084 McGwire, K., Muscheler, R., Nishiizumi, K., Pasteris, D. R., Rhodes, R. H., and Sowers, T. A.:
1085 The WAIS Divide deep ice core WD2014 chronology – Part 2: Annual-layer counting (0–
1086 31 ka BP), Clim. Past, 12, 769–786, https://doi.org/10.5194/cp-12-769-2016, 2016.

1087 Tcherkez, G. and Farquhar, G. D.: On the 16O/18O isotope effect associated with
1088 photosynthetic O2 production, Functional Plant Biol., 34, 1049,
1089 https://doi.org/10.1071/FP07168, 2007.

1090 Stolper, D. A., Fischer, W. W., and Bender, M. L.: Effects of temperature and carbon
1091 source on the isotopic fractionations associated with O2 respiration for 17O/16O and

18O/16O ratios in E. coli, Geochim. Cosmochim. Acta, 240, 152–172, https://doi.org/10.1016/j.gca.2018.07.039, 2018.

Veres, D., Bazin, L., Landais, A., Toyé Mahamadou Kele, H., Lemieux-Dudon, B., Parrenin, F., Martinerie, P., Blayo, E., Blunier, T., Capron, E., Chappellaz, J., Rasmussen, S. O., Severi, M., Svensson, A., Vinther, B., and Wolff, E. W.: The Antarctic ice core chronology (AICC2012): an optimized multi-parameter and multi-site dating approach for the last 120 thousand years, Clim. Past, 9, 1733–1748, https://doi.org/10.5194/cp-9-1733-2013, 2013.

Vilović, I., Schulze-Makuch, D., and Heller, R.: Variations in climate habitability parameters and their effect on Earth's biosphere during the Phanerozoic Eon, Sci Rep, 13, 12663, https://doi.org/10.1038/s41598-023-39716-z, 2023.

Vinogradov, A. P., Kutyurin, V. M., and Zadorozhnyi, I. K.: Isotope fractionation of atmospheric oxygen, Geochem. Int., 3, 241–253, 1959.

Von Caemmerer, S. and Farquhar, G. D.: Some relationships between the biochemistry of photosynthesis and the gas exchange of leaves, Planta, 153, 376–387, https://doi.org/10.1007/BF00384257, 1981.

Waelbroeck, C., Kiefer, T., Dokken, T., Chen, M.-T., Spero, H. J., Jung, S., Weinelt, M., Kucera, M., Paul, A., Bintanja, R., van de Wal, R. S. W., and Oerlemans, J.: Constraints on surface seawater oxygen isotope change between the Last Glacial Maximum and the Late Holocene, *Quat. Sci. Rev.*, 24, 835–852, https://doi.org/10.1016/j.quascirev.2004.03.006, 2005.

Wang, Y., Cheng, H., Edwards, R. L., Kong, X., Shao, X., Chen, S., Wu, J., Jiang, X., Wang, X., and An, Z.: Millennial- and orbital-scale changes in the East Asian monsoon over the past 224,000 years, Nature, 451, 1090–1093, https://doi.org/10.1038/nature06692, 2008.

West, J. B., Sobek, A., and Ehleringer, J. R.: A Simplified GIS Approach to Modeling Global Leaf Water Isoscapes, PLoS ONE, 3, e2447, https://doi.org/10.1371/journal.pone.0002447, 2008.

Wostbrock*, J. A. G. and Sharp, Z. D.: Triple Oxygen Isotopes in Silica–Water and Carbonate–Water Systems, Reviews in Mineralogy and Geochemistry, 86, 367–400, https://doi.org/10.2138/rmg.2021.86.11, 2021.

Wurgaft, E., Musan, I., Rivlin, T., and Luz, B.: Weak isotopic fractionation of dissolved $O_2$ during community respiration, *Limnol. Oceanogr.*, 67, 1794–1804, https://doi.org/10.1002/lno.12167, 2022.

# *Appendice*

# Air oxygen fractionation associated with respiration and photosynthesis processes in plants: impact on the study of the global Dole effect

Clémence Paul[1], Clément Piel[2], Joana Sauze[2], Ji-Woong Yang[1], Marie Bouchet[1], Olivier Jossoud[1], Arnaud Dapoigny[1], Daniele Romanini[4], Frédéric Prié[1], Sébastien Devidal[2], Roxanne Jacob[1], Alexandru Milcu[2,3] and Amaëlle Landais[1]

[1] Laboratoire des Sciences du Climat et de l'Environnement (LSCE/IPSL/CEA/CNRS/UVSQ/UPS), UMR 8212, Gif-sur-Yvette, France

[2]Ecotron Européen de Montpellier (UAR 3248), Univ Montpellier, Centre National de la Recherche Scientifique (CNRS), Campus Baillarguet, Montferrier-sur-Lez, France

[3]Centre d'Ecologie Fonctionnelle et Evolutive, Univ Montpellier, CNRS, Univ Paul Valéry, EPHE, IRD, Montpellier, France

*Correspondence to:* Clémence Paul (clemence.paul@lsce.ipsl.fr)

a)

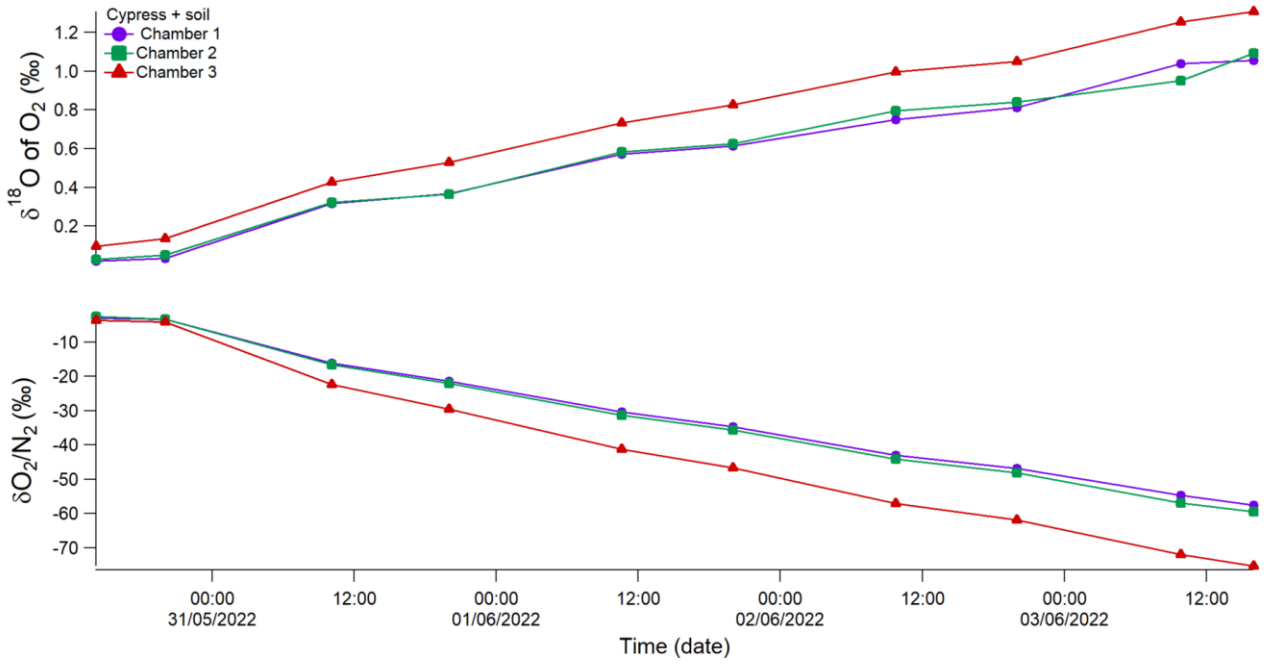
Cypress + soil
Chamber 1
Chamber 2
Chamber 3
δ18O of O2 (‰)
1.2
1.0
0.8
0.6
0.4
0.2
δO2/N2 (‰)
-10
-20
-30
-40
-50
-60
-70
00:00
31/05/2022
12:00
00:00
01/06/2022
12:00
00:00
02/06/2022
12:00
00:00
03/06/2022
12:00
Time (date)

b)

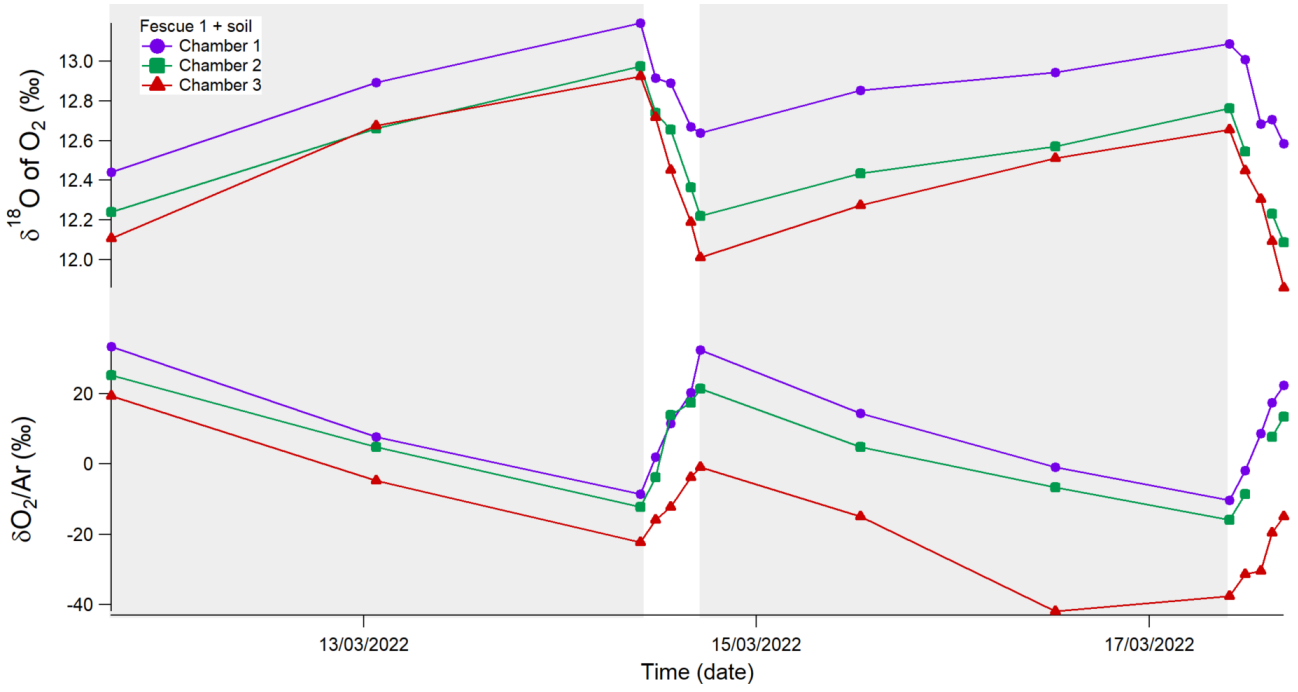


1172

1173

1174 c)

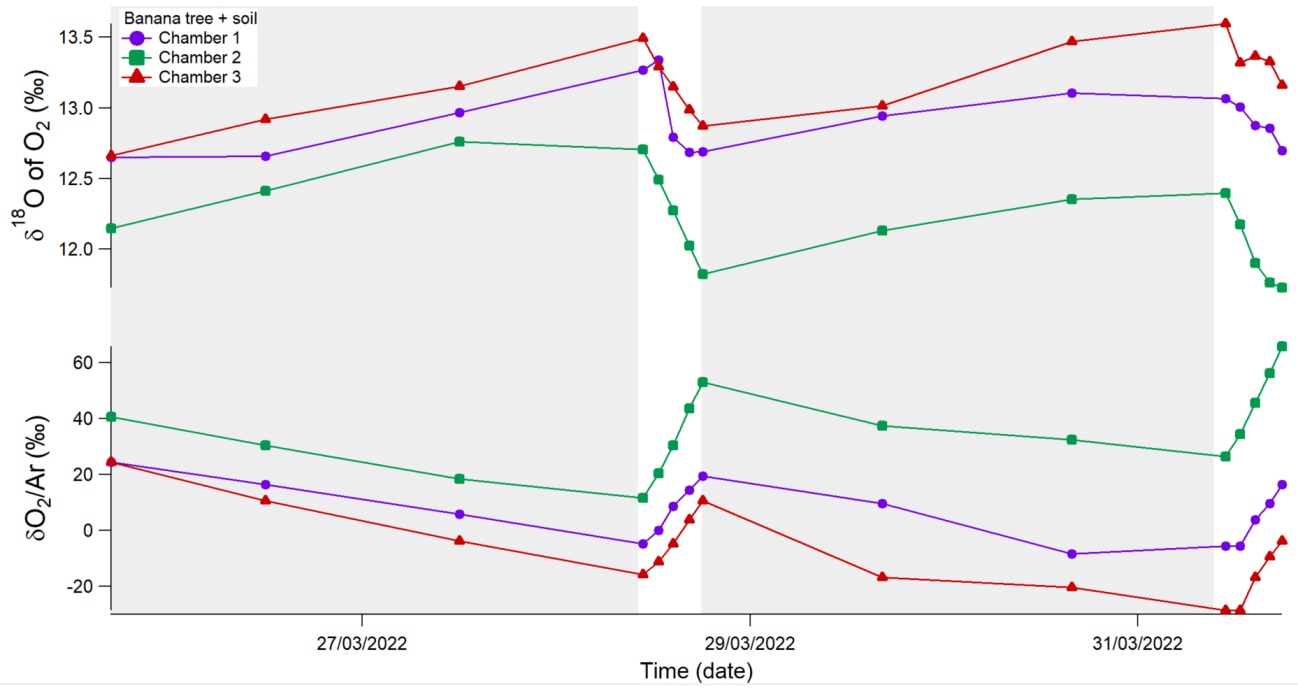


1175

1176 d)

1177

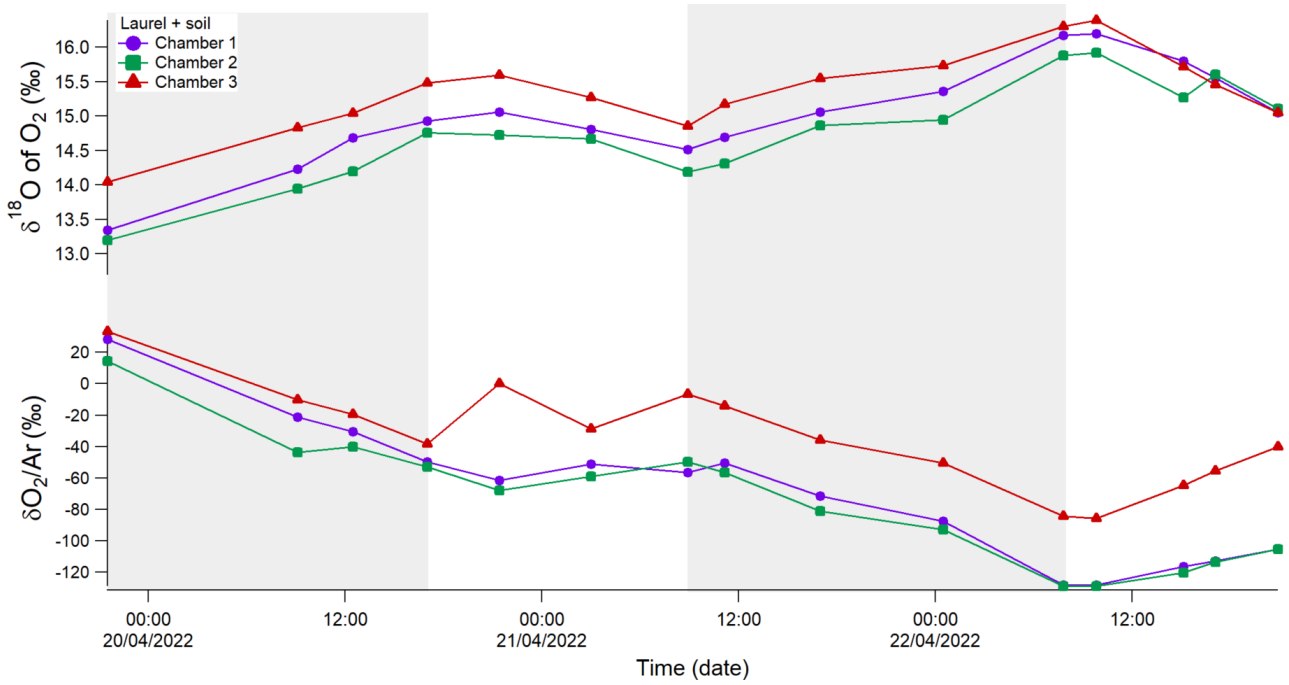


1178

1179

1180

1181 *Fig.A1 Evolution of the different isotope ratios analyzed by IRMS from four experiments with different plants and soil*
1182 *resulting from respiration in the dark and photosynthesis during light periods in three closed chambers simultaneously*
1183 *over several days. Gray rectangles correspond to dark periods and white rectangles to light periods. (a) corresponds to the*
1184 *Cypress dark-only experiment, (b) corresponds to the first day/night experiment for fescue, (c) for banana tree, (d) for*
1185 *Laurel. The top of the graphs corresponds to variations in $\delta^{18}O$ of $O_2$ and the bottom to variations in $\delta O_2/Ar$. Purple with*
1186 *dots: evolution of $\delta^{18}O$ of $O_2$ and $\delta O_2/Ar$ for chamber 1. Green with rectangles: evolution of $\delta^{18}O$ of $O_2$ and $\delta O_2/Ar$ for*
1187 *chamber 2. Red with triangles: evolution of $\delta^{18}O$ of $O_2$ and $\delta O_2/Ar$ for chamber 3*.

1188

1189 a)

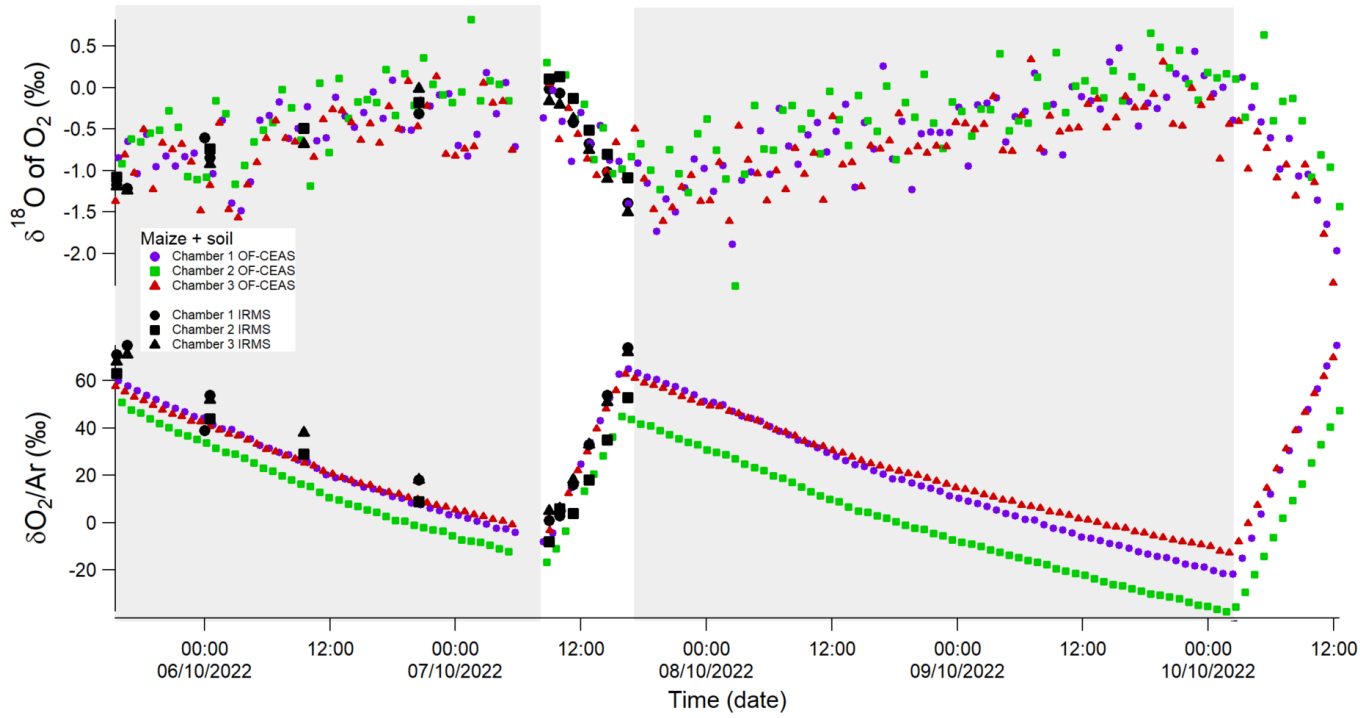
δ18O of O2 (‰)
0.5
0.0
-0.5
-1.0
-1.5
-2.0
Maize + soil
Chamber 1 OF-CEAS
Chamber 2 OF-CEAS
Chamber 3 OF-CEAS
Chamber 1 IRMS
Chamber 2 IRMS
Chamber 3 IRMS
δO2/Ar (‰)
60
40
20
0
-20
00:00
06/10/2022
12:00
00:00
07/10/2022
12:00
00:00
08/10/2022
12:00
00:00
09/10/2022
12:00
00:00
10/10/2022
12:00
Time (date)

b)

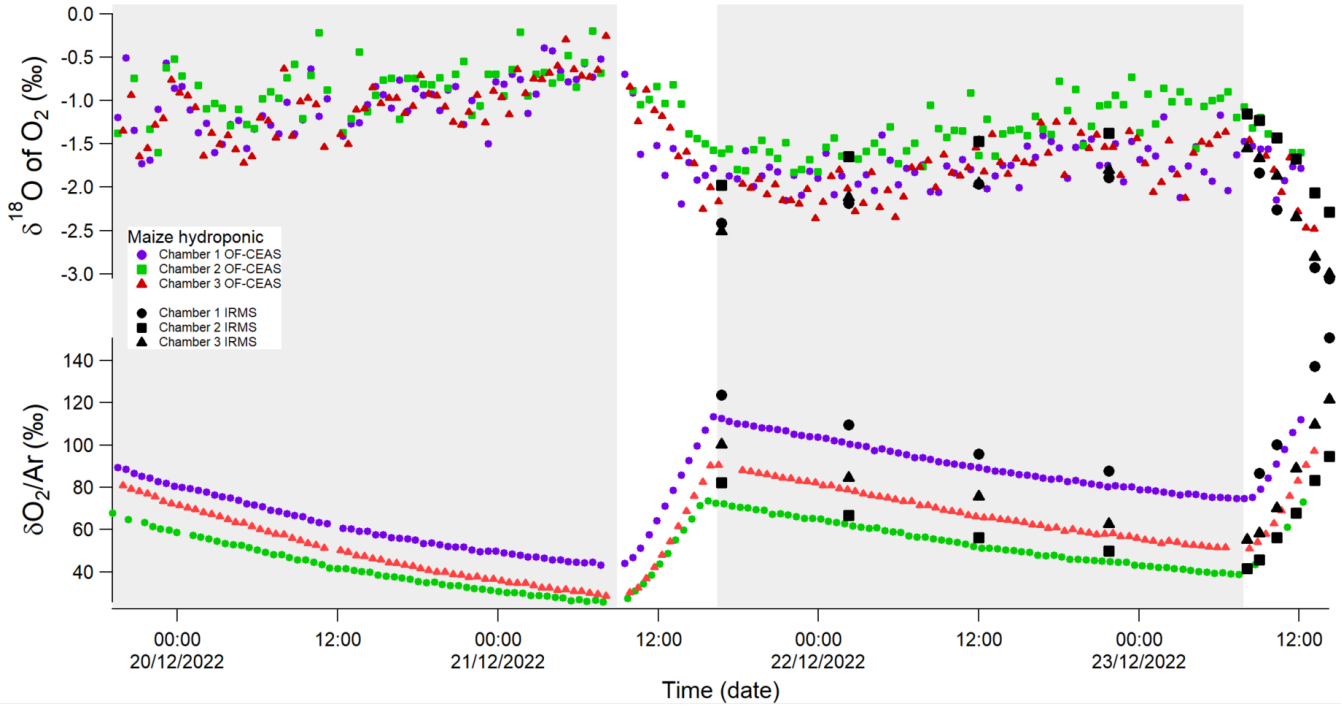
δ18O of O2 (‰)
0.0
-0.5
-1.0
-1.5
-2.0
-2.5
-3.0
Maize hydroponic
Chamber 1 OF-CEAS
Chamber 2 OF-CEAS
Chamber 3 OF-CEAS
Chamber 1 IRMS
Chamber 2 IRMS
Chamber 3 IRMS
δO2/Ar (‰)
140
120
100
80
60
40
00:00
20/12/2022
12:00
00:00
21/12/2022
12:00
00:00
22/12/2022
12:00
00:00
23/12/2022
12:00
Time (date)

c)

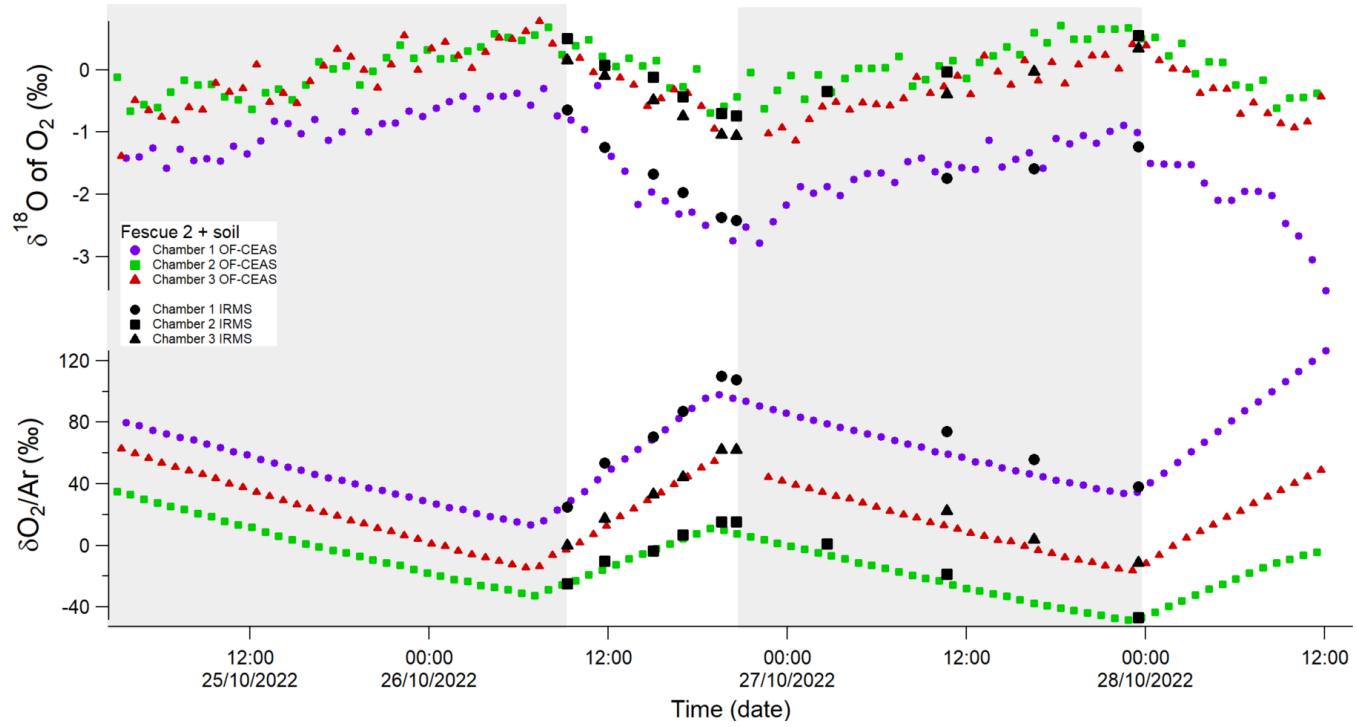


1218

1219

1220

1221

1222 d)

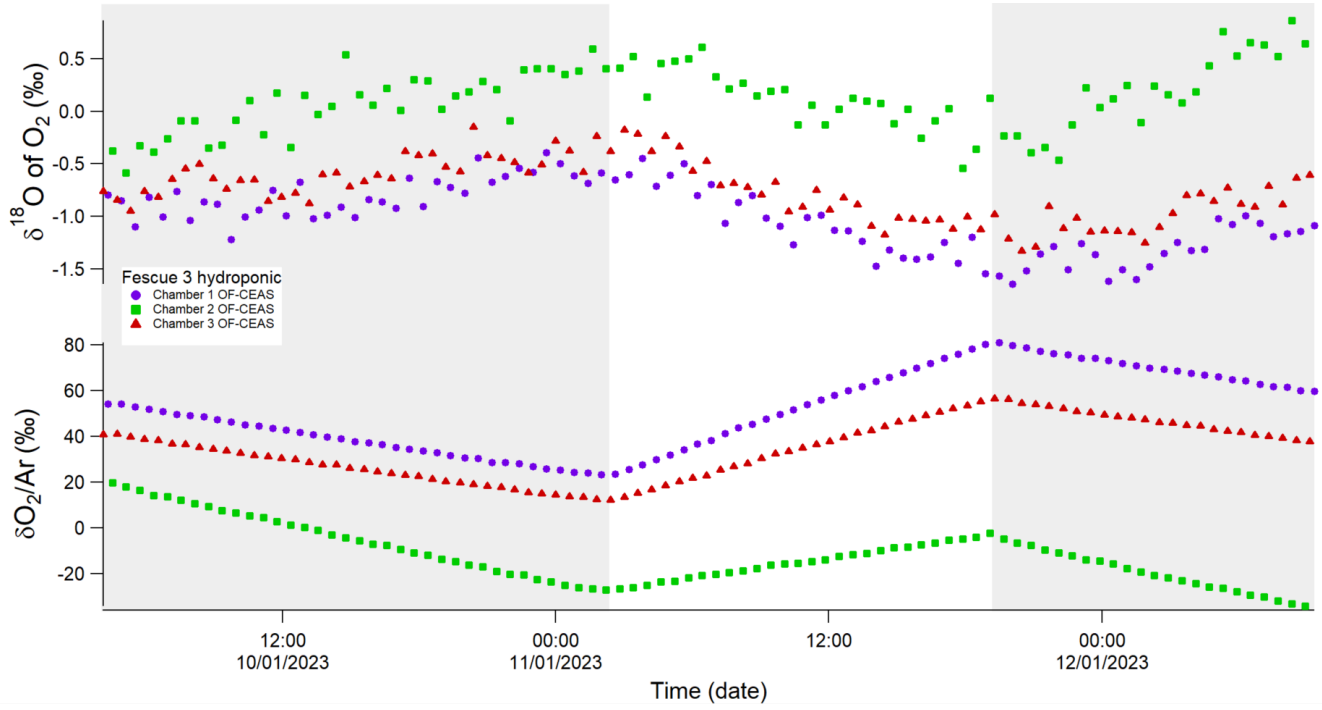


1223

e)

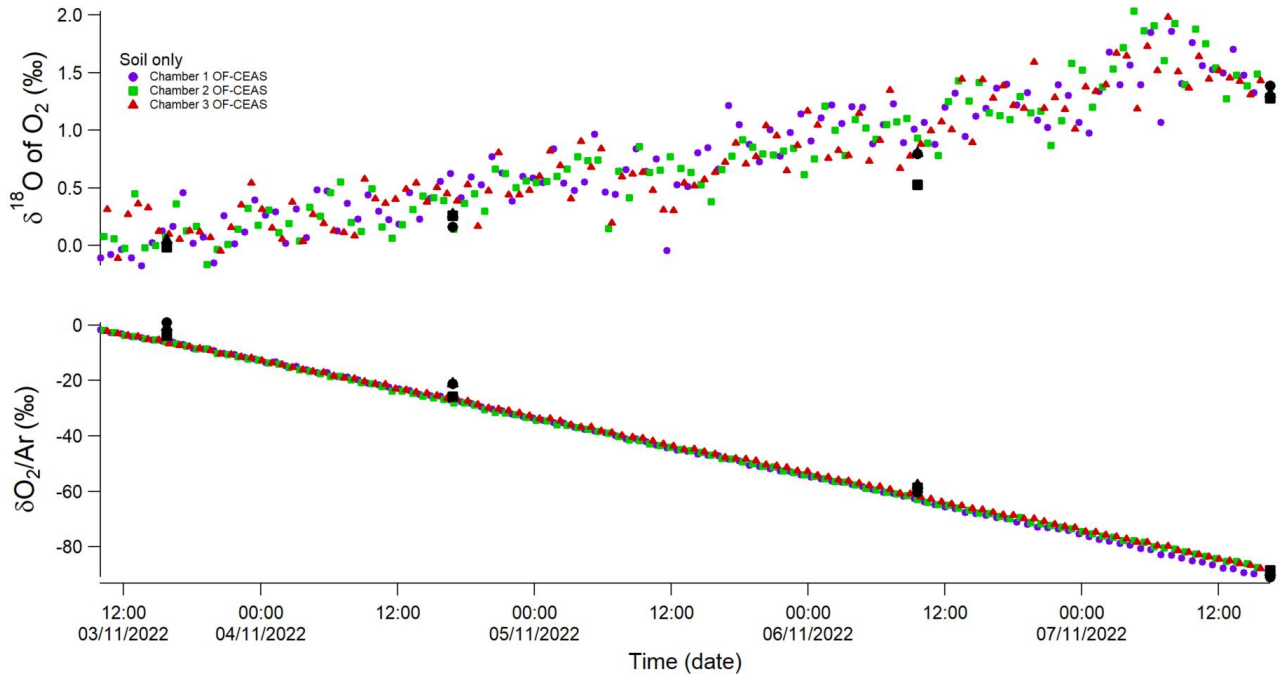


*Fig.A2 Evolution of the different isotope ratios analyzed by IRM and OF-CEAS techniques simultaneously from five experiments with different plants and soil resulting from respiration in the dark and photosynthesis during light periods in three closed chambers simultaneously over several days. Gray rectangles correspond to dark periods and white rectangles to light periods. (a) corresponds to the Maize and soil experiment during light and dark periods, (b) corresponds to the Maize in hydroponic conditions, (c) corresponds to the second fescue and soil experiment, (d) corresponds to the third fescue experiment in hydroponic conditions and (e) corresponds to soil only. The top of the graphs corresponds to variations in $\delta^{18}O$ of $O_2$ and the bottom to variations in $\delta O_2/Ar$. The coloured graphs correspond to the analysis via the OF-CEAS technique: in purple with the circles: evolution of $\delta^{18}O$ of $O_2$ and $\delta O_2/Ar$ for chamber 1. In green with the rectangles: evolution of $\delta^{18}O$ of $O_2$ and $\delta O_2/Ar$ for chamber 2. In red with the triangles: evolution of $\delta^{18}O$ of $O_2$ and $\delta O_2/Ar$ for chamber 3. Figures in black correspond to analysis via IRMS: chamber 1 (dot), chamber 2 (rectangle), chamber 3 (triangle).*

*Table A1. $\alpha_{photosynthesis}$ values obtained from sensitivity tests with respect to different fractionation factors associated with dark respiration*

| Plant | $^{18}\varepsilon_{dark\_respi-}$ (‰) | $^{18}\varepsilon_{photosynthesis}$ (‰) |
|---|---|---|

| | | |
|---|---|---|
| Fescue + soil | -18 | 4.7 |
| | -40 | 0.2 |
| | -50 | -1.8 |

1243

1244

1245 *Table A2. $\alpha_{photosynthesis}$ value obtained from sensitivity test against a 2 ‰ decrease in $\delta^{18}O_{lw}$ value*

| Plant | $\delta^{18}O_{lw}$ (‰) | $^{18}\varepsilon_{photosynthesis}$ (‰) |
|---|---|---|
| Fescue + soil | -25.5 (measured) | 4.7 |
| | -23.5 | 3.0 |

1246

1247

1248

1249 *Table A3. Global Dole simulated with the IPSL-CM5A-LR model at PI: sensitivity to different $\alpha_{photosynthesis}$ and $^{18}\varepsilon_{dark\_respi}$*
1250 *values*

| IPSL-CM5A-LR at PI | $^{18}\varepsilon_{photosynthesis}$ (‰) | $^{18}\varepsilon_{dark\_respi}$(‰) | Global DE (‰) |
|---|---|---|---|
| This study | 3.7 | 17 | 25.5 |
| | 13.3 | 17 | 32.9 |
| | 3.7 | 16 | 24.7 |
| | 3.7 | 21 | 28.6 |

1251

1252